

# Interrelations between coeval mafic and A-type silicic magmas from composite dykes in a bimodal suite of southern Israel, northernmost Arabian–Nubian Shield: Geochemical and isotope constraints

Y. Katzir<sup>a</sup>, B.A. Litvinovsky<sup>a,\*</sup>, B.M. Jahn<sup>b</sup>, M. Eyal<sup>a</sup>, A.N. Zanzilevich<sup>a</sup>,  
J.W. Valley<sup>c</sup>, Ye. Vapnik<sup>a</sup>, Y. Beerl<sup>a</sup>, M.J. Spicuzza<sup>c</sup>

<sup>a</sup> Department of Geological and Environmental Sciences, Ben Gurion University of the Negev, Beer Sheva 84105, Israel

<sup>b</sup> Institute of Earth Sciences, Academia Sinica, Taipei 11529, Taiwan

<sup>c</sup> Department of Geology and Geophysics, University of Wisconsin, Madison WI 53706, USA

Received 30 September 2006; accepted 3 January 2007

Available online 13 January 2007

## Abstract

Late Neoproterozoic bimodal dyke suites are abundant in the Arabian–Nubian Shield. In southern Israel this suite includes dominant alkaline quartz porphyry dykes, rare mafic dykes, and numerous composite dykes with felsic interiors and mafic margins. The quartz porphyry chemically corresponds to A-type granite. Composite dykes with either abrupt or gradational contacts between the felsic and mafic rocks bear field, petrographic and chemical evidence for coexistence and mixing of basaltic and rhyolitic magmas. Mixing and formation of hybrid intermediate magmas commenced at depth and continued during emplacement of the dykes. Oxygen isotope ratios of alkali feldspar in quartz porphyry (13 to 15‰) and of plagioclase in trachydolerite (10–11‰) are much higher than their initial magmatic ratios predicted by equilibrium with unaltered quartz (8 to 9‰) and clinopyroxene (5.8‰). The elevation of  $\delta^{18}\text{O}$  in alkali feldspar and plagioclase, and extensive turbidization and sericitization call for post-magmatic low-temperature ( $\leq 100\text{ }^\circ\text{C}$ ) water–rock interaction. Hydrous alteration of alkali feldspar, the major carrier of Rb and Sr in the quartz–porphyry, also accounts for the highly variable and unusually high I(Sr) of 0.71253 to 0.73648.

The initial  $^{143}\text{Nd}/^{144}\text{Nd}$  ratios, expressed by  $\varepsilon_{\text{Nd}}(T)$  values, are probably unaltered and show small variation in mafic and felsic rocks within a narrow range from +1.4 to +3.3. The Nd isotope signature suggests either a common mantle source for the mafic and silicic magmas or a juvenile crustal source for the felsic rocks (metamorphic rocks from the Elat area). However, oxygen isotope ratios of zircon in quartz porphyry [ $\delta^{18}\text{O}(\text{Zr})=6.5$  to  $7.2\text{‰}$ ] reveal significant crustal contribution to the rhyolite magma, suggesting that mafic and A-type silicic magmas are not co-genetic, although coeval. Comparison of  $^{18}\text{O}/^{16}\text{O}$  ratios in zircon allows to distinguish two groups of A-type granites in the region: those with mantle-derived source,  $\delta^{18}\text{O}(\text{Zr})$  ranging from 5.5 to 5.8‰ (Timna and Katharina granitoids) and those with major contribution of the modified juvenile crustal component,  $\delta^{18}\text{O}(\text{Zr})$  varying from 6.5 to 7.2‰ (Elat quartz porphyry dykes and the Yehoshafat alkaline granite). This suggests that A-type silicic magmas in the northern ANS originated by alternative processes almost coevally.

© 2007 Elsevier B.V. All rights reserved.

**Keywords:** Composite dyke; A-type granite; Oxygen isotopes; Sr isotopes; Nd isotopes; Arabian–Nubian shield

\* Corresponding author.

E-mail address: [borisl@bgu.ac.il](mailto:borisl@bgu.ac.il) (B.A. Litvinovsky).

## 1. Introduction

Composite dykes that are made up of felsic and mafic rocks are abundant worldwide (e.g., Vogel and Wilband, 1978; Marshall and Sparks, 1984; Furman and Spera, 1985; Stern and Voegeli, 1987; Carrigan and Eichelberg, 1990; Poli and Tommazzini, 1991; Koyaguchi and Takada, 1994; Litvinovsky et al., 1995a; Titov et al., 2000; Jarrar et al., 2004). Composite dykes, like microgranular mafic enclaves (MME) and synplutonic basic dykes in felsic igneous rocks, provide unequivocal evidence for coexistent magmas of contrasting composition. Comparative study of mafic and felsic rocks in composite dykes can shed light on possible genetic links between mafic magmas and contemporaneous silicic melts. In post-orogenic settings the felsic rocks of composite dykes exhibit geochemical traits of A-type granite, so the felsic rocks may serve as one of key objects for study of the origin of A-type granites (Stern and Voegeli, 1987; Jarrar et al., 2004).

Two different types of composite dykes are distinguished (Snyder et al., 1997; Wiebe and Ulrich, 1997): (Type 1) those with felsic margins and mafic interiors; the latter are commonly in the form of pillow-like and rounded enclaves or as a net-veined essentially mafic dykes; (Type 2) dykes with felsic interiors and mafic margins; a main distinctive feature of these dykes is clear zoning with smooth planar contacts, both abrupt and gradational, between felsic interior and mafic marginal zones.

Type 1 dykes are less appropriate for reconstruction of the initial magma compositions due to the high extent of interaction between the commingling magmas. This particularly affects the more mobile elements such as K, Rb, Na, Ba, Ca, Sr (Zorpi et al., 1991; Poli and Tommazzini, 1991; Litvinovsky et al., 1995b). It is also known that exchange of radiogenic isotopes between two co-eval magmas occurs much faster than element diffusion (Snyder and Tait, 1998; and references therein). This causes ambiguity in the study of consanguinity of coeval mafic and silicic melts and sources of mafic magmas.

Type 2 composite dykes provide more reliable information on the chemical composition of coexisting magmas. The dykes are thought to form in shallow level plutonic or subvolcanic systems when basaltic melts ruptured a granitic magma reservoir and injected country rocks forming dykes outside the reservoir; silicic magma flowed outward in the center of basaltic dyke prior to its complete solidification (Gibson and Walker, 1963; Kanaris-Sotiriou and Gill, 1985; Wiebe and Ulrich, 1997). Depending on the time interval between the two

successive injections, contacts between felsic interiors and mafic margins vary from clearly gradational to abrupt. Abrupt contacts, common in many dykes, suggest that interaction of two magmas was inhibited due to the high extent of crystallization of the earlier mafic magma. In composite dykes with gradational contacts the initial composition of mafic rocks could be preserved at least in the outermost parts where the injected mafic melt solidified rapidly adjacent to cold country rocks.

Composite dykes of type 2 are abundant in the northernmost part of the Arabian–Nubian shield (ANS), in particular in the Eastern Desert and Sinai (Egypt), in southwestern Jordan and in southern Israel (Stern and Voegeli, 1987, 1995; Beyth et al., 1994; Iacumin et al., 1998; Mushkin et al., 1999, 2003; Jarrar et al., 2004). These dykes are incorporated in bimodal basalt–rhyolite dyke suites forming dyke swarms up to tens of kilometers long. The felsic rocks are chemically referred to as typical A-type granite (Stern et al., 1988; Kessel et al., 1998; Mushkin et al., 2003). Dykes are shown to be genetically linked to bimodal volcanic suites of similar composition (Stern et al., 1988; Jarrar et al., 1992).

Here we present new data on the structure, and the geochemical and isotope characteristics of the trachy-dolerite–quartz porphyry bimodal dyke suite in southern Israel including composite dykes both with abrupt and gradational contacts between felsic and mafic zones. Particular emphasis has been placed on the magma mixing process and its effect on the original chemical composition of the rocks. Comparison of oxygen and Sr isotope data suggests that the Rb–Sr isotope system had been significantly disturbed by low-temperature water–rock interaction and, consequently, the measured  $^{87}\text{Sr}/^{86}\text{Sr}$  ratios do not characterize the magmatic process. Despite having similar  $\epsilon_{\text{Nd}}(T)$  the felsic and mafic rocks are not cogenetic:  $\delta^{18}\text{O}$  values of zircon indicate significant contribution of upper crustal sources to the A-type rhyolite magma.

## 2. Geological setting

The study was performed in the Elat area, the largest exposure of Precambrian basement in southern Israel. Along with the adjacent Amram and Timna exposures, as well as a number of outcrops in Jordan, the Elat area represents the northernmost edge of the ANS (Fig. 1, Inset). The shield formed during the Neoproterozoic (ca. 900–550 Ma) as part of the East African Orogen by accretion of juvenile arc terranes. The accretion occurred at  $\sim 700$  Ma (Stern, 1994 and references therein) and was followed by

continental collision that resulted in magmatic thickening by intrusion of large calc-alkaline granitic batholiths (Stoeser and Camp, 1985). The batholithic stage (stage 3 of Bentor, 1985) lasted from ~650 Ma until 620–610 Ma. The stage ended with regional uplifting and erosion at ~610–600 Ma and formation of molasse deposits (Garfunkel, 2000; Jarrar et al., 2003). Late Neoproterozoic crustal evolution (ca. 610–540 Ma) in the ANS occurred in an extensional tectonic environment (Stern and Hedge, 1985; Bentor and Eyal, 1987; Stern et al., 1988; Baer et al., 1994; Garfunkel, 2000; Genna et al., 2002) and was accompanied by abundant igneous activity: emplacement of alkaline granitoids, eruption of bimodal volcanics, and intrusion of dyke swarms, also mostly bimodal (Stern et al., 1984; Stern and Gottfried, 1986; Beyth et al., 1994; Jarrar et al., 1992, 2004; Stein et al., 1997; Jarrar, 2001; Moghazi, 2002).

In southern Israel basement outcrops comprise metamorphic and magmatic rocks that represent all of the main stages of the ANS evolution (Bentor, 1985; Garfunkel et al., 2000). The Late Neoproterozoic stage included deposition of molasse (Elat conglomerate), formation of bimodal alkaline plutonic complexes (Timna and Amram complexes) and andesite–rhyolite volcanism (for geological map see Supplementary data, Fig. 1S).

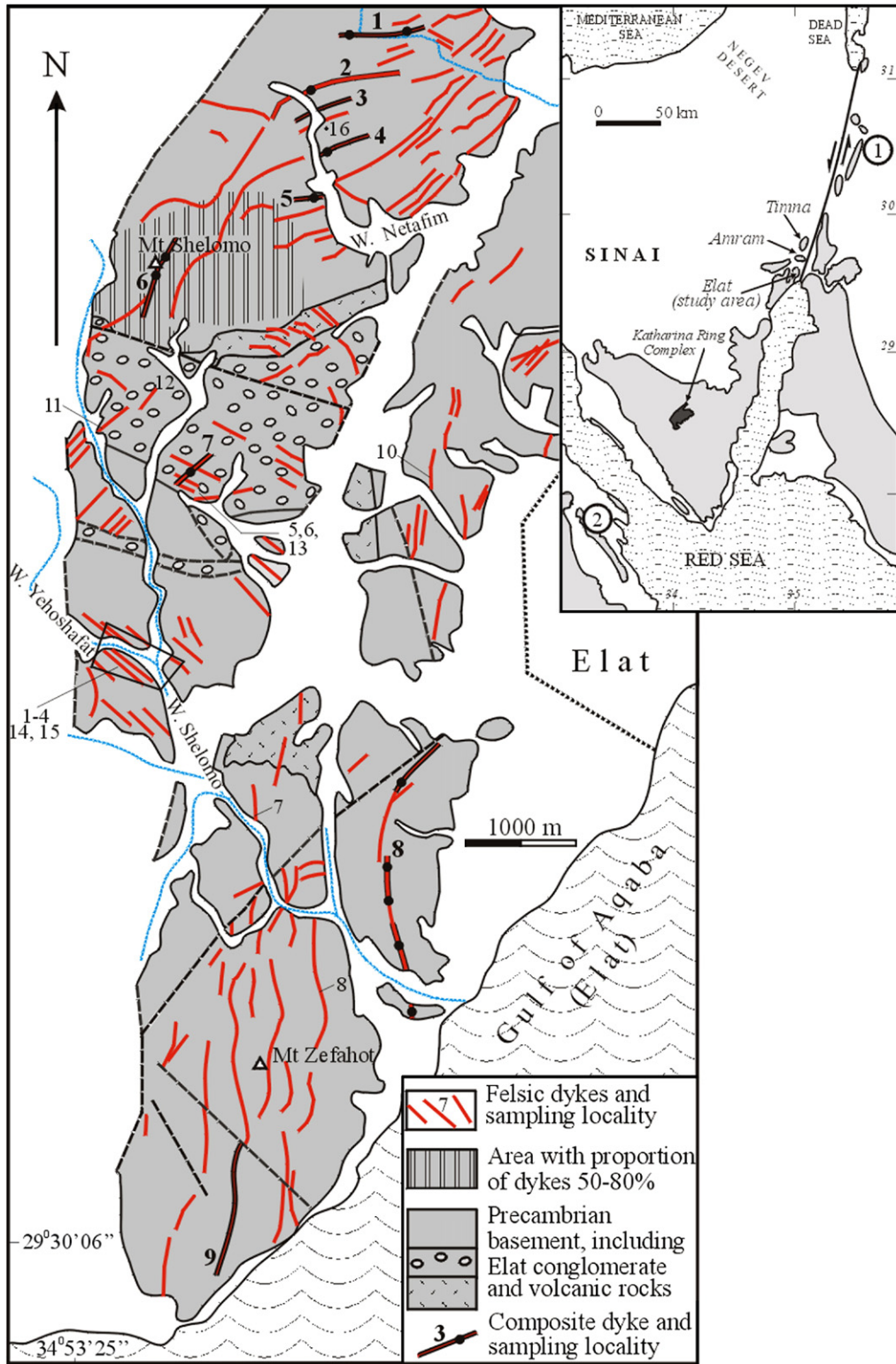
Four successive dyke episodes were widely exhibited in southern Israel during the second half of the Neoproterozoic, from ~615 Ma to 530 Ma (Katzir et al., 2006): (1) Microdiorite and lamprophyre dyke suite; (2) Dacite porphyry with subordinate andesite and rhyolite porphyry; (3) Bimodal dyke suite, rhyolites with small amount of trachydolerite and intermediate rocks, mostly in composite dykes; (4) Dolerite, commonly high-Ti. Dyke episodes 1, 2 and 3 were separated in time by plutonic, volcanic and sedimentation events. The first two suites are timed to the very end of the batholithic stage; they are overlain by Elat conglomerate formed at ~600 Ma (Garfunkel, 2000). Dykes of the bimodal suite and the youngest dolerite dykes intrude all Neoproterozoic igneous and sedimentary rocks (Kessel et al., 1998; Beyth and Heimann, 1999; Katzir et al., 2006).

The bimodal dyke suite is the most abundant among the Neoproterozoic dykes in southern Israel (Fig. 1). The schematic map of the dykes was compiled based on aerial photograph interpretation; however, field observa-

tions showed that in a number of localities in central and northern Elat area the number of dykes is an order of magnitude higher. In the vicinity of Mt. Shelomo, within an area of about 1 by 2 km they constitute 50 to 80% of the total rock volume (Gutkin and Eyal, 1998). The general trend of the dykes is predominantly NS and changes gradually to N50°E in the northern part of the area. In the upper reaches of Wadi Shelomo two trends of dykes are distinguished: N40°W and N30°E. The dykes are few hundred meters to 3 km long, commonly vertical and steeply dipping. Their thickness ranges from 1 to 30 m. In larger dykes, en echelon arrayed segments, commonly 0.5–1 km long, are observed. Felsic rocks, mostly quartz porphyry, are absolutely dominant in the suite. The proportion of mafic rocks in the bimodal suite in southern Israel is approximately 5 vol.%. Trachydolerite and trachyandesite dykes are rare; instead, mafic rocks constitute margins in composite dykes that are part of the bimodal dyke suite. About a dozen of such dykes were found in the Elat area (Fig. 1), and several dykes were mapped immediately to the north, in the Amram and Timna exposures (Beyth et al., 1994; Mushkin et al., 1999). Along-strike tracing of some larger quartz porphyry dykes often reveals sections with mafic margins. For instance, in dyke #8 that extends over 2.5 km several sections with mafic margins of about 1 m wide and 100–600 m long were observed (Fig. 1). This suggests that the real number of composite dykes may be larger than the dozen mapped ones.

The composite dykes are mostly subvertical, up to 2.5 km long and commonly 10 to 20 m wide. The felsic interiors consist of homogeneous quartz porphyry, but in some dykes they are contaminated by mafic material. The dyke margins are made up of trachydolerite, trachyandesite, and trachydacite. In places the composition of the mafic rocks changes along strike from andesite to dacite. The proportion of mafic rocks in a composite dyke is generally  $\leq 20\%$ . Contacts between the felsic interiors and mafic margins are commonly abrupt, without obvious signs of magma–magma interaction, but also without evidence of chilling (Fig. 2A). In few dykes the contact is highly gradational with heterogeneous mixing between the mafic and silicic magmas (Fig. 2B); in some dykes abrupt contact changes along strike to gradational, then back to abrupt (dyke #1 in Fig. 1).

Fig. 1. Distribution of quartz porphyry, rhyolite porphyry and composite dykes from the bimodal suite in the Elat area (based on an aerial photographs interpretation performed by V. Voznesensky, with authors' refinements). Area with abundant dykes, after Gutkin and Eyal (1998). Cretaceous to recent sedimentary sequences (undivided) are shown in white. Inset: 1 and 2 are Late Neoproterozoic bimodal volcanic and dyke suites in southwestern Jordan (Jarrar et al., 2004) and Northeastern Desert, Egypt (Stern et al., 1988).



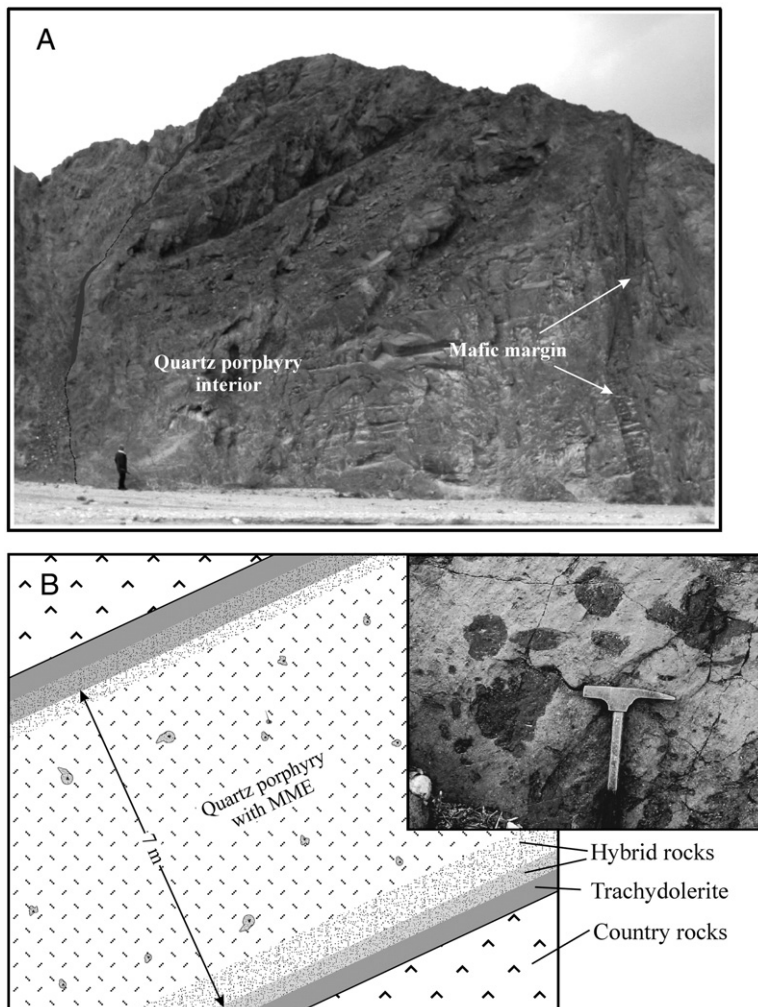


Fig. 2. Composite dykes of the second type in the Elat area. A, sub vertical 20-m wide composite dyke with abrupt contact between felsic interior and mafic margins. The dyke is exposed in Wadi Shehoret, 5 km to the north from the area shown in Fig. 1 (for locality, see Supplementary data). The left contact, highlighted by black line is subjected to tectonic fracturing. B, sketch of the structure of a composite dyke with gradational contacts between felsic interior and mafic margins (Fig. 1, dyke #2). The width of hybrid zones (30–50 cm) is off scale. The inset shows a photograph of typical microgranular mafic enclaves (MME) in quartz porphyry.

Evidence of commingling and mixing of basaltic and rhyolitic magmas is pictorially manifested in the composite Netafim dyke #2 located in the upper reaches of Wadi Netafim (Fig. 2B). Its thickness ranges from about 7 to 12 m including trachydolerite margins of 0.4–0.9 m wide. The contact between the quartz porphyry interior and trachydolerite margins is gradational, with two symmetrical transitional zones of about 30–50 cm in width. The transitional zones, in turn, are divided into two subzones. In the section adjacent to the quartz porphyry, the color of the rock progressively changes from brick red to reddish gray and has trachydacitic composition. In the section adjacent to the mafic margin the hybrid rock has dark reddish green color and

trachyandesitic composition. A blurred transition zone between the hybrid trachydacite and trachyandesite can be easily traced for a distance of several tens of meters throughout the outcrop. Quartz porphyry of the interior of the Netafim dyke contains numerous, but unevenly distributed fine-grained, oval, rounded and irregular MME (Inset in Fig. 2B). Enclaves range from few millimeters to 20–25 cm across and have crenulate, sinuous, lobate and convex outlines. The curved shape of some enclaves points to plastic and ductile deformation. Also small mafic schlieren are fairly common throughout the quartz porphyry. This shows that the central zone of the Netafim dyke shares some traits of Type 1 composite dykes.

The stratigraphic position and age of the bimodal dyke suite is constrained by field relations: dykes intrude all Late Neoproterozoic plutonic, volcanic and sedimentary rock units, including a volcanic suite made up of alkaline rhyolite and andesite (Mushkin et al., 2003). In turn, they are intersected by dolerite dykes dated to  $531 \pm 5$  Ma in the Timna area ( $^{40}\text{Ar}/^{39}\text{Ar}$ ; Beyth and Heimann, 1999), and to  $545 \pm 13$  Ma in southwestern Jordan (K–Ar; Jarrar, 2001). The dated dolerite dyke from Timna is overlain by Early Cambrian sandstone (Beyth and Heimann, 1999).

Recent U–Pb dating of zircon grains of quartz porphyry and trachydolerite from composite dyke #2 (Fig. 2B) yielded ages of  $592.7 \pm 6$  Ma and  $593.7 \pm 8.4$  Ma, respectively, which are consistent with the magmas being coeval (Y. Beeri; in situ ion probe analysis in the NORDSIM Facility, Swedish Museum of National History, Stockholm). The analytical procedures and results will be described in detail in a special paper. The U–Pb zircon ages are similar to a Rb–Sr whole rock age of Late Neoproterozoic bimodal swarm and composite dykes in the Northeastern Desert and Sinai Peninsula, Egypt (Stern and Hedge, 1985; Stern and Voegeli, 1987, 1995).

The 593 Ma U–Pb age of the bimodal dyke suite is in conflict with an age estimate for volcanic rhyolites in southern Israel, 550 Ma, which is based on a Rb–Sr isochron (Bielski, 1982). Our study of rhyolites from the localities sampled by Bielski (Moon Valley, northern Ramat–Yotam caldera, Amram area) showed that ultra-K rhyolites with  $\text{K}_2\text{O}$  content ranging from 8 to 10 wt.% are widespread in these areas. The highly unusual composition of the rocks was attributed to extensive metasomatic alteration that resulted in dramatic increase of potassium on the expense of sodium (Agron and Bentor, 1981). Below, in Section 7.4, significant disturbance of the Rb–Sr system, even in rhyolite dykes with minimal evidence of metasomatic alteration, is demonstrated. Therefore Rb–Sr dating of volcanic rhyolite in southern Israel is highly debatable. Since the dykes from the bimodal suites are considered as feeders for volcanics (Stern et al., 1988; Jarrar et al., 1992; Mushkin et al., 1999), the latter cannot be much older than the dyke rocks.

### 3. Analytical methods

Whole-rock chemical analyses were performed using a combination of wet chemical methods, atomic absorption spectroscopy and titration (major elements), and X-ray fluorescence (Rb, Sr, Ba, Y, Zr and Nb) at the Geological Institute, Siberian Division of the Russian

Academy of Sciences, Ulan-Ude. Rare earth and some selected trace elements (Hf, Ta, Th, U, Ga, V, Cu, Pb, Zn, Sc and Cs) were analyzed by the ICP-MS method at the National Taiwan University, Taipei and at the Institute of Mineralogy and Geochemistry of Rare Elements, Moscow. Analyses are considered accurate to within 2–5% for major elements, and better than 10–15% for trace elements. The accuracy for all the REE (except Lu) is 1–5%; for Lu, it is 9–10%.

Electron microprobe mineral analyses were carried out using a modernized four-channel MAR-3 electron probe microanalyser at the Geological Institute, Ulan-Ude. Analyses were obtained with a beam of 2–3  $\mu\text{m}$ . Operating conditions were 20 kV, 40  $\mu\text{A}$  beam current, and a counting time of 10 s. The detection limits are 0.05–0.09 wt.% for  $\text{Na}_2\text{O}$ ,  $\text{MgO}$ ,  $\text{Al}_2\text{O}_3$ , and  $\text{SiO}_2$ ; 0.01–0.05 wt.% for  $\text{K}_2\text{O}$ ,  $\text{CaO}$ ,  $\text{TiO}_2$ ,  $\text{MnO}$  and  $\text{FeO}$ .

For oxygen isotope analysis high purity mineral separates were hand picked from crushed and sieved rock samples. Zircon (2.5–3.5 mg per analysis) was separated from the 63–200  $\mu\text{m}$  size fraction using standard methods including Wilfley shaking table, Frantz magnetic separator and heavy liquids. Zircon concentrates were treated with a series of cold acids to remove potential contaminants. Purity of zircon separates was ensured by hand picking. Oxygen isotope analysis of minerals and whole-rock samples was performed using the laser fluorination technique at the University of Wisconsin — Madison (Valley et al., 1995).  $\text{BrF}_5$  was used as the reagent. Oxygen was purified cryogenically and with an inline Hg diffusion pump, converted to  $\text{CO}_2$  using a hot graphite rod, and analyzed on a Finnigan MAT 251 mass spectrometer. Quartz separates (1 to 1.5 mg per analysis) were analyzed using the rapid heating, defocused beam technique (Spicuzza et al., 1998a). Plagioclase and alkali feldspar separates and whole rock powders, which might react appreciably with  $\text{BrF}_5$  at room temperature, were analyzed (2 to 2.5 mg per analysis) using an ‘air-lock’ sample chamber, which allows fluorination of each sample individually (Spicuzza et al., 1998b). The long-term reproducibilities for conventionally lased samples and for samples lased in the ‘air-lock’ chamber in the UW isotope lab are 0.1 and 0.2‰, respectively. On each day of analysis at least four aliquots of UW Gore Mountain Garnet standard (UWG-2) were analyzed. The overall average for 29 analyses on six days of conventionally lased UWG-2 in this study is  $5.59 \pm 0.13\text{‰}$ . UWG-2 analyzed using the ‘air lock’ chamber averaged at  $5.57 \pm 0.18\text{‰}$  ( $n=36$ ). Data for each day of analysis were adjusted by an average of 0.21‰ (0.23‰ for ‘air-lock’ analysis days), determined by the difference between each

day's UWG-2 value and 5.8‰, the accepted  $\delta^{18}\text{O}$  (SMOW) value of UWG-2 (Valley et al., 1995).

*Rb–Sr and Sm–Nd isotope analyses.* Sr and Nd isotopic ratios were measured using a Finnigan MAT-262 thermal ionization mass spectrometer at the Institute of Earth Sciences (IES), Academia Sinica, Taipei. Concentrations of Rb, Sr, Sm and Nd were determined by ICP-MS using an Agilent 7500 s spectrometer at the

National Taiwan University. For concentration determination, fused glass beads were powdered and dissolved in HF/HNO<sub>3</sub> (1:1) mixture in capped Savilex beakers for >2 h at ca. 100 °C, followed by evaporation to dryness, then refluxing in 7N HNO<sub>3</sub> for >12 h at ca. 100 °C, and finally, diluting the sample solution by 2% HNO<sub>3</sub>. An internal standard solution of 5 ppb Rh and Bi was added and the spiked solution was further diluted

Table 1  
Chemical composition of representative rocks from simple dykes of the bimodal suite (wt.%, ppm)

Sample no.	A144-2	A149	A157	A150-1	A128	A129	A239	D59	A52	A90-4	D10	D16	D44	A147-2	A156-1	A200	A255
	1	2	3	4	5	6	7	8	9	10	11	12	13	14	15	16	17
SiO <sub>2</sub>	77.2	76.7	76.7	76.4	77.0	76.8	78.4	77.3	76.6	77.2	74.6	71.4	69.8	73.3	70.2	57.3	49.53
TiO <sub>2</sub>	0.1	0.13	0.15	0.13	0.1	0.12	0.1	0.1	0.12	0.09	0.24	0.36	0.44	0.2	0.39	1.09	2.02
Al <sub>2</sub> O <sub>3</sub>	11.7	11.3	11.3	11.1	11.9	11.7	10.1	11.3	11.4	10.85	12.4	12.8	13.2	12.95	14.55	17.6	15.1
Fe <sub>2</sub> O <sub>3</sub>	1.97	2.05	2.85	1.85	1.65	1.76	1.98	2.7	1.8	1.49	1.18	3.0	3.34	2.47	2.74	2.65	8.11
FeO	0.11	0.07	0.07	0.19	0.15	0.22	0.11		0.16	0.19	0.36	0.2	0.37	0.15	0.11	3.47	3.32
MnO	0.06	0.02	0.02	0.01	0.01	0.01	0.02	0.01	0.01	0.01	0.05	0.05	0.03	0.06	0.04	0.09	0.14
MgO	0.06	0.14	0.17	0.23	0.29	0.18	0.05	0.2	0.22	0.39	0.25	0.48	1.45	0.3	0.61	3.15	4.46
CaO	0.14	0.32	0.01	0.55	0.48	0.37	0.48	0.3	0.1	0.48	0.12	1.30	0.98	0.38	0.44	2.09	4.7
Na <sub>2</sub> O	3.41	3.57	2.72	3.46	3.9	3.6	2.65	3	3.6	3.2	2.78	3.62	3.71	5.11	5.19	5.50	5.65
K <sub>2</sub> O	4.92	4.86	5.48	5.0	4.08	4.24	5.3	5	4.65	4.81	6.36	4.45	4.66	4.0	4.08	3.58	1.15
P <sub>2</sub> O <sub>5</sub>	–	0.05	–	0.05	–	–	–	0.05	–	–	–	0.06	0.08	0.05	0.10	0.29	0.49
LOI	0.39	0.82	0.74	0.82	0.56	0.86	0.43		0.62	1.48	0.98	1.56	1.91	0.50	1.08	2.76	4.74
Total	100.06	100.03	100.21	99.79	100.12	99.86	99.62	99.96	99.28	100.19	99.32	99.29	99.97	99.47	99.53	99.57	99.41
Rb	150	170	190	170	140	140	180	150	220	170	150	95	90	84	96	97	15
Sr	27	40	55	43	13	21	38	40	49	67	30	70	85	25	96	470	380
Ba	190	94	180	180	70	55	200	190	210	120	300	250	300	760	840	780	520
Nb	33	36	34	35	29	32	31	27	32	33	34	38	29	18	16	3	17
Ta	7.41			3.7	3.62			6.6			6	6	2.9	1.94	2.23		
Th	17			15.2	15.4		17							9.4	10.5		
U	5.61			5.02	4.14									3.52	3.49		
Zr	590	600	570	630	600	550	560		550	640		410	400	390	360	210	240
Hf	13.7			13.3	13.2									7.7	7.8		
Y	68	70	68	75	78	76	64	55	70	75	47	43	30	37	31	26	35
Ga	21			16	20									17	17		
La	39			27	29			30			34	36	35	32	17		22
Ce	89			79	69			85			70	65	80	88	66		76
Pr	10.6			8.6	8.7			7.2			8.2	8.5	9.2	8.4	4.7		
Nd	41			35	35			28			33	35	37	32	20		28
Sm	9.8			8.7	8.8			7.8			7.4	7.7	7	6.2	5		
Eu	0.18			0.2	0.14			0.09			0.6	0.6	0.56	0.82	0.87		
Gd	9.4			9.1	8.8			8.2			7	7	5.7	5.2	4.9		
Tb	1.63			1.55	1.53			1.5			1.3	1.3	0.95	0.83	0.84		
Dy	10.3			10.2	9.8			9.4			7.6	7.1	5.6	5.2	5.1		
Ho	2.31			2.23	2.18			1.9			1.6	1.5	1.1	1.17	1.13		
Er	6.32			6.07	6.01			5.9			4.7	4.5	3.3	3.18	3.1		
Tm	0.95			0.91	0.9			0.95			0.67	0.64	0.53	0.49	0.46		
Yb	5.92			5.72	5.65			5.9			4.4	4.3	4.4	3.08	3.03		
Lu	0.9			0.84	0.83			0.79			0.69	0.7	0.46	0.49	0.47		
Eu/Eu*	0.06			0.07	0.05			0.03			0.25	0.25	0.27	0.44	0.54		
La <sub>n</sub> /Yb <sub>n</sub>	4.8			3.4	3.7			3.7			5.5	6	5.7	7.4	4.1		
(Na+K)/Al	0.93	0.98	0.92	1	0.91	0.9	1	0.92	0.96	0.96	0.92	0.84	0.84	0.98	0.89		

(1) Samples 1–10 = quartz porphyry, 11–12 = feldspathic rhyolite porphyry, 13 = trachyandesite, 14 = trachydolerite.

(2) Eu/Eu\* = Eu<sub>n</sub>/(Sm<sub>n</sub>\*Gd<sub>n</sub>)<sup>1/2</sup>; (Na+K)/Al, agpaitic index = (Na<sub>2</sub>O+K<sub>2</sub>O)/Al<sub>2</sub>O<sub>3</sub>, mol.%.

(3) Here and in Tables 2 and 3 hyphen = concentration of element below the detection limit.

(4) Sampling localities are shown in Fig. 1; sample A255 from Amram area.

Table 2  
Chemical composition of representative rocks from composite dykes (CD) of the bimodal suite (wt.%, ppm)

Sample no.	A260-6	A197-1	A202	A198	D218a	D231	A127	A127-1	A30	A66-3	A18	A285	A260-1	A260-3	A260-4	A196-1	N-1	A197-8	A197-7	A202-2	A202-1	A198-1	D21aa	A127-2	A141-1	D62-1			
# of CD in Fig. 1	CD-1	CD-2	CD-4	CD-5	CD-6		CD-7		CD-8			CD- Anram	CD-1			CD-2				CD-4		CD-5	CD-6	CD-7	CD-8				
	<i>Quartz porphyry from interiors</i>												<i>Mafic rocks from marginal zones</i>																
SiO <sub>2</sub>	68.61	71.7	76.2	73.8	73.4	72.3	74.1	73.2	76	76.2	74.7	74.6	56.6	62.2	66.7	50.8	52.8	61.3	65.5	61.7	64.1	49.3	50.47	55.0	65.4	60.9			
TiO <sub>2</sub>	0.46	0.33	0.2	0.29	0.28	0.28	0.25	0.35	0.16	0.13	0.14	0.2	1.14	0.82	0.61	1.83	1.72	1.04	0.67	1.15	1.06	2.88	2.77	2.17	1.03	1.36			
Al <sub>2</sub> O <sub>3</sub>	13.55	13	12.05	12.4	12.35	12.6	11.6	11.8	11.6	11.6	11.2	11.8	16.9	15.4	14	15.3	14.7	13.9	13.3	14.65	14.65	14.7	14.75	14.0	13.8	14.25			
Fe <sub>2</sub> O <sub>3</sub>	2.67	0.76	1.78	2.65	2.22	4.22	2.99	2.66	2.79	2.74	2.6	2.12	4.62	3.63	2.36	3.44	4.82	2.02	1.65	3.08	2.06	6.57	11.56	9.9	5.1	6.44			
FeO	0.92	1.81	0.16	0.26	0.46	0.23	0.34	0.72	0.32	0.18	0.16	0.13	2.69	1.96	1.78	4.35	4.1	3.14	2.12	2.25	2.09	4.35	–	1.17	0.53	0.78			
MnO	0.05	0.04	0.01	0.02	0.04	0.04	0.03	0.03	–	0.01	–	0.02	0.07	0.06	0.06	0.17	0.18	0.11	0.08	0.07	0.04	0.14	0.1	0.08	0.05	0.08			
MgO	1.57	0.56	0.13	0.2	0.42	0.58	0.92	0.79	0.05	0.13	–	0.34	2.65	2.22	1.49	4.47	4.6	2.5	1.1	2.7	2.27	4.99	4.37	3.77	2.32	2.65			
CaO	1.11	0.85	0.26	0.44	0.78	0.4	0.49	0.53	0.48	0.19	1.13	0.24	2.35	1.68	1.39	6.28	6.0	3.82	3.04	1.93	2.0	4.3	3.2	2.89	1.73	2.1			
Na <sub>2</sub> O	5.46	2.75	3.85	3.86	3.25	3.36	3.55	3.34	4.6	3.0	3.72	2.88	5.51	5	4.65	3.79	3.27	3.5	2.51	3.47	4.3	3.83	3.32	4.28	3.58	4.16			
K <sub>2</sub> O	4.04	6.34	4.92	5.11	5.89	5.35	4.0	4.77	3.0	5.4	3.88	5.84	4.61	4.74	5.18	3.2	2.76	4.44	5.97	5.26	4.19	3.22	3.36	2.07	3.72	3.25			
P <sub>2</sub> O <sub>5</sub>	0.15	0.06	–	–	–	–	–	0.05	–	–	–	–	0.33	0.23	0.2	0.38	0.4	0.2	0.12	0.39	0.33	1.07	1.19	0.52	0.25	0.35			
LOI	1.33	1.9	0.58	0.44	1.19	1.26	1.64	1.26	0.83	0.82	2.12	1.33	2.65	2.21	1.64	5.44	4.65	4.23	3.41	2.84	2.53	5.02	5.05	4.37	2.2	3.46			
Total	99.92	100.1	100.14	99.8	100.28	100.62	99.91	99.5	99.83	100.4	99.75	99.5	100.12	100.15	100.06	99.45	100	100.2	99.47	99.49	99.62	100.37	100.14	100.22	99.71	99.78			
Rb	100	145	140	115	130	120	91	120	95	194	135	150	107	100	120	86	65	92	140	150	115	73	102	52	130	92			
Sr	300	110	72	81	52	52	41	56	30	60	50	56	360	390	320	460	430	310	190	200	160	400	167	140	130	140			
Ba	670	460	280	240	450	320	60	70	50	150	50	240	800	900	1130	940	750	490	690	740	460	840	657	430	460	640			
Nb	10	25	20	30	28	29	45	51	32	34	35	30	7	9	11	13	18	19	21	14	13	14	22	26	23	23			
Ta				4.71			3.54	4.15	4.13	2.75	3.01					1.17	0.57						1.47	1.01					
Th				11.5	13	11	12.7	11.6	17.5	17.7	17.3	16				4.2	3.7						4.5	5.8					
U				3.69			3.92	3.76	4.46	5.75	4.74					1.15	0.81						1.49	1.91					
Zr	190	430	270	470	390	440	620	660	590	590	590	410	225	180	190	210	220	320	370	360	370	280	318	350	420	390			
Hf				11.3			14.3	14.1	14.1	14.4	14					5.2	4.7						6.8	8.2					
Y	19	37	42	63	37	53	74	75	64	75	68	44	24	21	19	28	26	35	35	54	52	45	48	51	51	48			
Ga				17	21	20	28	23	23	19	21	20				23	20						34	27					
La		56		42	59	48	61	60	28	43	60	58				24	28	37	43				34	40					
Ce		117		94	110	95	132	131	65	102	120	106				52	58	84	94				82	90					
Pr		15		11.3			15.1	15.9	7.2	12.2	14					7.1	6.8	11.1	12.4				11	11.3					
Nd		58		47	58	43	59	63	32	50	55	43				30	28	44	48				50	48					
Sm		10.4		10.3			11.9	12.4	9	11.6	11.5					6.1	5.6	8.7	9.2				11.0	9.9					
Eu		0.64		0.73			0.66	0.72	0.2	0.28	0.3					1.5	1.58	1.18	0.92				3.19	2.19					
Gd		10.7		9.5			11.4	11	8.5	11	11					6.4	5.2	9.0	9.6				10.1	8.9					
Tb		1.34		1.58			2	1.76	1.7	1.93	1.9					0.8	0.81	1.17	1.2				1.53	1.35					
Dy		7		8.8			11.2	10.7	10.3	11.2	11					4.2	4.7	6.2	6.6				7.9	8					
Ho		1.35		1.77			2.24	2.3	2.2	2.33	2.3					0.8	0.94	1.18	1.26				1.5	1.68					
Er		4.18		4.99			6.38	6.19	6.9	6.73	6.9					2.35	2.6	3.48	3.77				3.95	4.26					
Tm		0.65		0.74			0.94	0.93	1	1.02	0.98					0.33	0.37	0.52	0.58				0.53	0.62					
Yb		4.15		4.93			6.11	5.81	6.7	6.57	6.5					1.96	2.45	3.26	3.65				3.37	3.86					
Lu		0.64		0.76			0.92	0.87	1	0.98	0.98					0.29	0.37	0.51	0.56				0.48	0.57					
Eu/Eu*		0.19		0.23			0.17	0.19	0.07	0.08	0.08					0.74	0.89	0.41	0.3				0.92	0.71					
La <sub>n</sub> /Yb <sub>n</sub>		9.7		6.1			7.2	7.4	3	4.7	6.6					8.8	8.3	8.1	8.4				7.3	7.5					
(Na+K)/Al	0.98	0.88	0.97	0.96	0.95	0.9	0.88	0.9	0.93	0.93	0.92	0.94																	

Eu/Eu\* = Eu<sub>n</sub> / (Sm<sub>n</sub> \* Gd<sub>n</sub>)<sup>1/2</sup>; (Na+K)/Al, agpaitic index = (Na<sub>2</sub>O + K<sub>2</sub>O)/Al<sub>2</sub>O<sub>3</sub>, mol.%.

2000 times with 2% HNO<sub>3</sub> before ICP-MS analysis. The internal standard was used for monitoring the signal shift during the measurement. The analytical precision was about ±3% (2σ). Sr and Nd isotopic compositions were analyzed on unspiked samples. Powdered samples were dissolved in Savilex bombs and followed by a series of standard procedures until samples were completely dissolved. Isolation of Sr and Nd were achieved using a 2-column technique, and Sr fractions were occasionally further purified using a third column. The first column was packed with 2.5 ml cation exchange resin (Bio-Rad AG50W-X8, 100–200 mesh) and was used to collect Sr and REE fractions. The second column used for Sr purification was packed with 1 ml cation exchange resin, identical to the above. The second column used for Nd isolation was packed with 1 ml Ln-B25-A (Eichron) resin, which was covered on top by a thin layer of anion exchange resin (Bio-Rad AG1-X8, 200–400 mesh). Mass analyses were performed using a 7-collector Finnigan MAT-262 mass spectrometer in dynamic mode. <sup>143</sup>Nd/<sup>144</sup>Nd ratios were normalized against the value of <sup>146</sup>Nd/<sup>144</sup>Nd=0.7219, whereas <sup>87</sup>Sr/<sup>86</sup>Sr ratios were normalized to <sup>86</sup>Sr/<sup>88</sup>Sr=0.1194. During the course of analyses, measurements on NBS-987 Sr standard yielded <sup>87</sup>Sr/<sup>86</sup>Sr=0.710320±0.000036 (*n*=50) using static mode); and =0.710237±0.000020 (*n*=8) using dynamic mode. The <sup>87</sup>Sr/<sup>86</sup>Sr ratios reported herein (Table 5) have been duly adjusted

to NBS-987 = 0.710250. Our measurements on La Jolla Nd standard yielded 0.511864±0.000006 (*n*=4), and on JMC Nd standard, 0.511821±0.000016 (*n*=6). The one-stage model age (*T*<sub>DM-1</sub>) is calculated assuming a linear Nd isotopic growth of the depleted mantle reservoir from ε<sub>Nd</sub>(*T*)=0 at 4.56 Ga to +10 at the present time.

$$T_{DM-1} = 1/\lambda \ln \left\{ 1 + \left[ \left( \frac{^{143}\text{Nd}}{^{144}\text{Nd}} \right)_s - 0.51315 \right] / \left[ \left( \frac{^{147}\text{Sm}}{^{144}\text{Nd}} \right)_s - 0.2137 \right] \right\},$$

where *s*=sample, λ=decay constant of <sup>147</sup>Sm (0.00654 Ga<sup>-1</sup>).

The two-stage model age (*T*<sub>DM-2</sub>) is obtained assuming that the protolith of the granitic magmas has a Sm/Nd ratio (or *f*<sub>Sm/Nd</sub> value) of the average continental crust (Keto and Jacobsen, 1987)

$$T_{DM-2} = T_{DMI} - (T_{DMI} - t)(fcc - fs) / (fcc - f_{DM}),$$

where fcc, fs, *f*<sub>DM</sub>=*f*<sub>Sm/Nd</sub> are values of the average continental crust, the sample and the depleted mantle, respectively. In our calculation, fcc=-0.4 and *f*<sub>DM</sub>=0.08592 are used, and *t*=the intrusive age of granite.

#### 4. Petrography

Quartz porphyry and subordinate feldspathic rhyolite porphyry are grayish pink and brick red homogeneous porphyritic rocks, with very fine-grained and

Table 3

Composition of rocks collected in the cross section through the Netafim composite dyke # 2 (wt.%, ppm)

Sample no.	A196-1	N-1	A196-2	A197-8	A197-7	N-6	N-2	A197	A197-1	A197-4	A197-5	N-7/1	A196-3	A197-6
Rock	TD	TD	TA	TA	Tdc	Tdc	QP	QP	QP	TDc	TA	TA	TA	TD
	1	2	3	4	5	6	7	8	9	10	11	12	13	14
SiO <sub>2</sub>	50.8	52.8	55.2	61.3	65.5	67.2	71.7	72.1	71.7	66.4	61.5	58.2	59.7	49.6
TiO <sub>2</sub>	1.83	1.72	1.54	1.04	0.67	0.7	0.3	0.32	0.33	0.63	1.09	1.26	1.23	2.15
Al <sub>2</sub> O <sub>3</sub>	15.3	14.7	14.6	13.9	13.3	13.0	12.7	13.3	13	13.2	14.1	13.95	14.5	15.6
Fe <sub>2</sub> O <sub>3</sub>	3.44	4.82	3.27	2.02	1.65	2.82	1.46	1.64	0.76	1.67	1.33	3.87	1.84	3.89
FeO	4.35	4.1	4.01	3.14	2.12	1.41	1.23	1.02	1.81	2.12	3.74	2.94	4.1	5.93
MnO	0.17	0.18	0.25	0.11	0.08	0.03	0.02	0.04	0.04	0.08	0.11	0.1	0.11	0.22
MgO	4.47	4.6	4.8	2.5	1.1	1.69	0.53	0.76	0.56	1.55	3.15	3.62	3.85	6.4
CaO	6.28	6.0	5.35	3.82	3.04	1.65	1.19	0.55	0.85	2.73	3.24	3.52	3.88	7.08
Na <sub>2</sub> O	3.79	3.27	3.76	3.5	2.51	3.21	2.38	3.71	2.75	2.96	3.51	3.62	3.46	3.74
K <sub>2</sub> O	3.78	2.76	3.09	4.44	5.97	5.66	6.6	5.19	6.34	5.65	4.61	4.3	3.5	1.73
P <sub>2</sub> O <sub>5</sub>	0.38	0.4	0.33	0.2	0.12	0.15	0.06	–	0.06	0.11	0.22	0.26	0.24	0.43
LOI	5.44	4.65	4.04	4.23	3.41	2.24	1.59	1.39	1.9	3.17	3.41	3.94	3.61	3.52
Total	100.03	100	100.24	100.2	99.47	99.76	99.76	99.99	100.1	100.27	100.01	99.58	100.02	100.29
Rb	86	65	72	92	140	140	160	105	145	135	100	98	69	37
Sr	460	430	410	310	190	170	150	105	110	230	290	340	330	560
Ba	940	750	670	490	690	370	530	240	460	500	540	590	420	560
Nb	13	18	15	19	21	32	37	26	25	22	21	20	19	12
Zr	210	220	240	320	370	380	440	430	430	380	310	270	280	200
Y	28	26	27	35	35	34	43	43	37	34	33	25	37	23

Abbreviations: TD = trachydolerite; TA = trachyandesite; Tdc = trachydacite; QP = quartz porphyry.

microcrystalline matrix. Phenocrysts of quartz, K-rich alkali feldspar and rare albite constitute up to 10 vol.%; in rhyolite porphyry quartz phenocrysts are absent. In rocks that contain mafic schlieren and microgranular enclaves some alkali feldspar phenocrysts are zoned: thin brown rim enriched in albitic component is clearly distinguished (Supplementary data, Table 1S). The matrix

of microgranophyric, cryptocrystalline and spherulitic texture is made up mainly of the same minerals as the phenocrysts; flakes of biotite and needles of iron oxides are evenly scattered. Accessories are zircon and apatite. The felsic dyke rocks are noticeably altered: biotite is almost completely replaced by hematite and chlorite, alkali feldspar phenocrysts are turbid, reddish brown, and

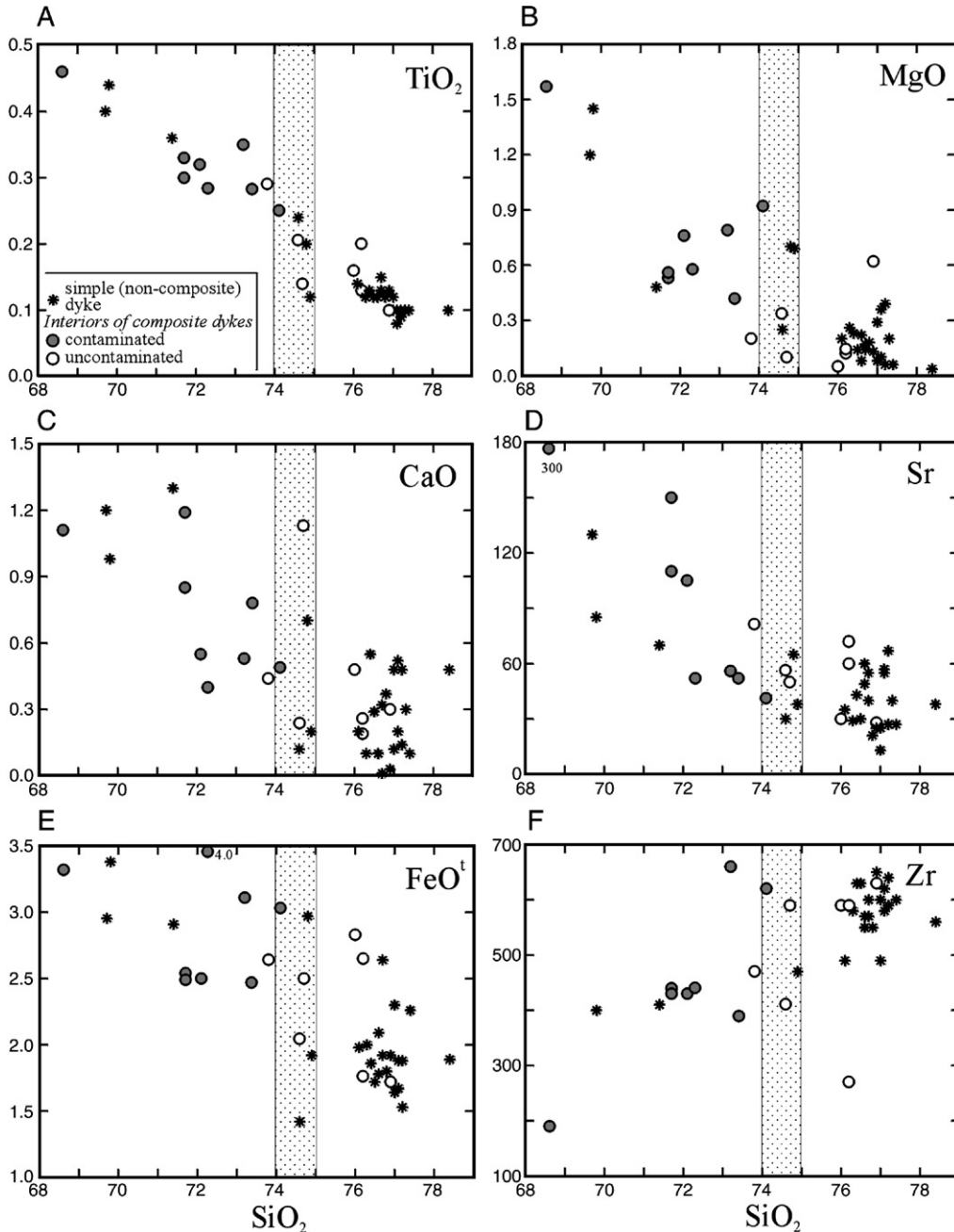


Fig. 3. Silica variation diagrams of selected major and trace elements in quartz porphyry dykes from the bimodal suite. Stippled bands designate the supposed border zone between "pure" and contaminated rocks.

spotty, and in the matrix alkali feldspar is partly replaced by clay minerals.

*Trachydolerite* is a dark gray, very fine-grained rock of porphyritic texture. Phenocrysts (3 to 5 vol.%) are elongated prisms of unzoned plagioclase ( $An_{52-54}$ , Table 1S) and subhedral crystals of augite enriched in Mg and Ca (Table 2S). The matrix is intragranular: wedge-shaped interstices between plagioclase laths ( $An_{41}$ ) are occupied by augite and Fe–Ti oxides. Interstitial alkali feldspar is a subordinate mineral (Table 1S). Other interstices are filled with hypocristalline aggregates of chlorite. Apatite is a common accessory mineral. The rock is considerably affected by alteration as indicated by the abundance of secondary chlorite, actinolite, carbonate, epidote and albite and by extensive sericitization of plagioclase.

*Trachyandesite and trachydacite* commonly bear evidence of hybrid origin. The hybrid rocks were studied in detail in the Netafim dyke #2 that shows gradational contacts between the felsic interior and mafic margins ('Geological setting'). The reddish gray trachydacite adjacent to the felsic interior has textural features and phenocryst population characteristic of quartz porphyry: euhedral quartz and alkali feldspar including grains with brown peripheral zones (Table 1S, samples A197-7 and A197-4). However, rare elongated plagioclase prisms, similar in shape to those in the trachydolerite, also occur. In the matrix, along with quartz and K-rich alkali feldspar, tiny plagioclase laths are observed.

The trachyandesite from the transitional zone is texturally similar to the adjacent trachydolerite, but along with andesine and augite phenocrysts (Tables 1S and 2S), xenocrysts of quartz and alkali feldspar are present. Alkali feldspars mostly occur as shapeless, heavily corroded relics. Quartz is commonly rimmed by pyroxene, which is compositionally distinct from magmatic augite (Table 2S, sample 197-5, phenocryst and rim). The matrix contains plagioclase ( $An_{28}$ ) and augite, with irregular grains of quartz and alkali feldspar. Their amount increases systematically towards the trachydacite subzone.

Trachyandesite and trachydacite making up marginal zones in composite dikes with abrupt contacts are often heterogenous. This is exhibited by the irregular variations of mafic and felsic mineral proportions at a distance of <1 m and by the occurrence of xenocrysts. Less common is homogenous trachyandesite that is similar in appearance and texture to trachydolerite.

## 5. Geochemistry

The geochemical data set contains 70 analyses. Of these, 26 samples were analyzed for rare earth elements

(REE). Data for representative samples are given in Tables 1, 2, and 3, and sampling localities are shown in Fig. 1. A full set of chemical data with sample localities is given in the online version of the Supplementary data (Table 3S, Fig. 2S).

*Quartz porphyry.* The chemical composition of quartz porphyry varies widely both in simple (non-composite) and composite dykes. In particular, silica content ranges from 68.6 to 78.4 wt.% (Fig. 3, Table 1). However, in the majority of samples from simple dykes the range is narrow extending from 76 to 77.5 wt.%  $SiO_2$ . By contrast, quartz porphyry making up the interiors of composite dykes is often less silica rich, with  $SiO_2 \leq 74$  wt.%. Decreased  $SiO_2$  content in felsic rocks is characteristic of varieties with clear textural and mineralogical evidence of contamination by mafic material (mafic enclaves and schlieren, plagioclase xenocrysts, alkali feldspar phenocrysts with brownish outer zones enriched in albite molecule). Contamination explains not only the  $SiO_2$ -depletion, but also the enrichments in MgO, FeO, CaO and related trace elements (Fig. 3) and the less pronounced negative Eu

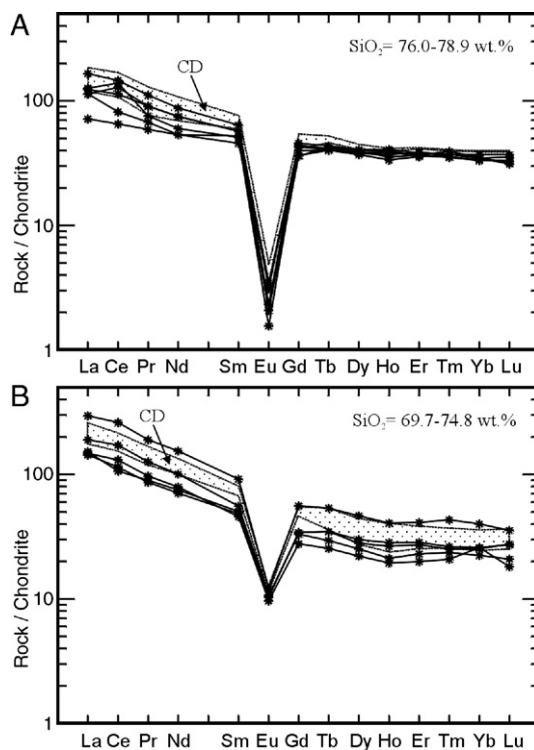


Fig. 4. Chondrite-normalized REE patterns for quartz porphyries from simple (non-composite) dykes (asterisks) and from composite dykes (CD), stippled area. A, "pure" quartz porphyry; B, contaminated quartz porphyry. Here and in Figs. 6 and 11 chondrite values are from Sun and McDonough (1989).

anomaly (Fig. 4A and B). In simple quartz porphyry dykes visible evidence of contamination is rare. However, the compositional similarity between homogenous silica-depleted quartz porphyry from simple dykes and undoubtedly contaminated rocks from composite dykes suggests that these dykes also crystallized from hybridized rhyolite magma. In Fig. 3 the border between “pure” and contaminated quartz porphyries is shown by convention at 74–75 wt.%  $\text{SiO}_2$ .

Uncontaminated (‘pure’) quartz porphyry corresponds chemically to alkaline granite (Fig. 5A and B) with apgaitic index of  $[\text{Na}+\text{K}]/\text{Al}>0.9$ , and  $\text{K}_2\text{O}$  (4.2–5.4 wt.%) dominating over  $\text{Na}_2\text{O}$  (Table 1). In the standard classification diagram (Marian and Piccoli, 1989) rock compositions occupy a small field straddling the border between metaluminous and peraluminous granites (not shown). Quartz porphyry exhibits geochemical traits of A-type granite (Fig. 5C) formed in a

within-plate environment (Fig. 5D). Major and trace element contents vary within narrow limits: the total content of  $\text{MgO}$ ,  $\text{CaO}$  and  $\text{TiO}_2$  is less than 1 wt.% and  $\text{FeO}^f = 1.5\text{--}2.6$  wt.% (Fig. 3). Average Zr and Y contents are fairly high, 570 and 69 ppm, respectively, whereas Sr content is low, 13–72 ppm (Tables 1 and 2, Figs. 3 and 5C).  $\Sigma\text{REE}$  averages 180 ppm, chondrite-normalized REE patterns are flat ( $\text{La}_n/\text{Yb}_n$  is about 3) and negative Eu anomaly is well pronounced, with  $\text{Eu}/\text{Eu}^*$  value of 0.05–0.07 (Tables 1 and 2; Fig. 4A).

Trachydolerite contains 47–53 wt.%  $\text{SiO}_2$ . It is low-Al ( $\text{Al}_2\text{O}_3 = 14.7\text{--}15.3$  wt.%) and low-Mg ( $\text{Mg}\# = 40\text{--}55$ ) with decreased  $\text{CaO}$  (3.2–6.3 wt.%). It is characterized by high contents of  $\text{Ba} = 660$  to 940 ppm,  $\text{Zr} = 210$  to 318 ppm, and  $\text{Y} = 26$  to 47 ppm (Table 2). Trachydolerites are classified according to their  $\text{TiO}_2$  content to moderate-Ti and high-Ti varieties, with 1.7–1.8 and 2.8–2.9 wt.%  $\text{TiO}_2$ , respectively. The two groups are similar in many

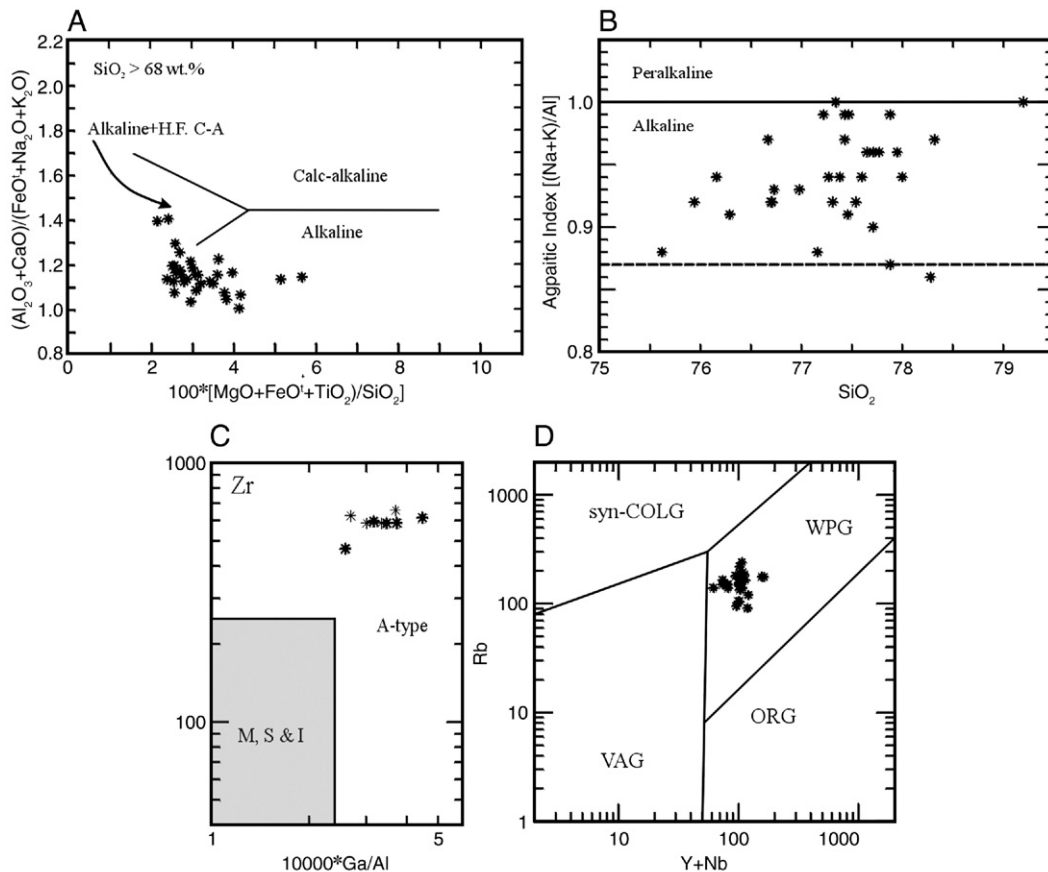


Fig. 5. Quartz porphyry compositions plotted in classification diagrams. A,  $100 * [(\text{MgO} + \text{FeO}^f + \text{TiO}_2) / \text{SiO}_2]$  vs  $(\text{Al}_2\text{O}_3 + \text{CaO}) / (\text{FeO}^f + \text{Na}_2\text{O} + \text{K}_2\text{O})$  diagram, after Sylvester (1989); H.F. C–A= highly fractionated calc-alkaline. B,  $\text{SiO}_2$  vs Apgaitic Index  $[(\text{Na} + \text{K}) / \text{Al}]$ , after Liégeois and Black (1987). C,  $\text{Ga} / \text{Al}$  vs Zr diagram; gray rectangles denote the fields of S-, I-, and M-type granitoids (after Whalen et al., 1987). D,  $\text{Y} + \text{Nb}$  vs Rb tectonic classification diagram, after Pearce et al. (1984).

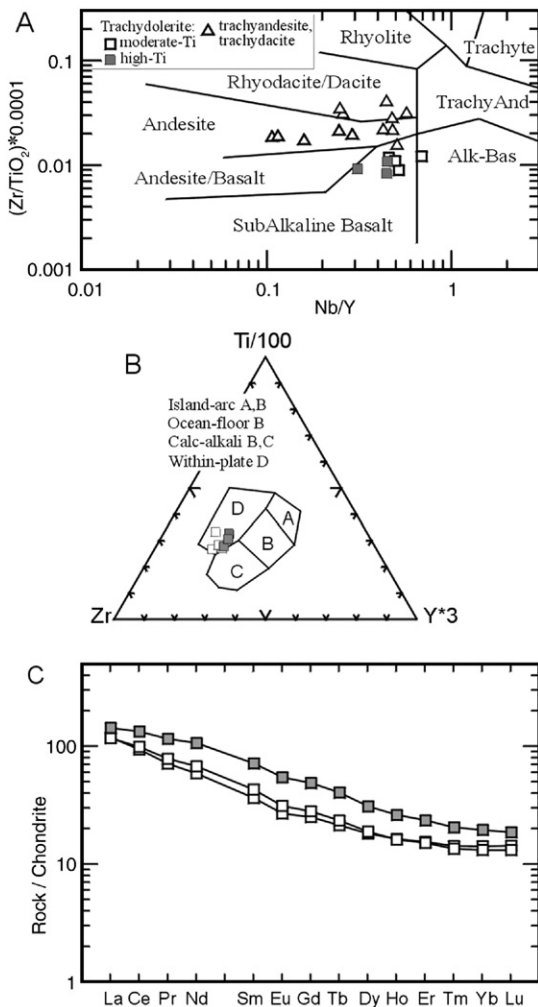


Fig. 6. Mafic rock compositions plotted in classification diagrams. A, Nb/Y vs  $[(Zr/TiO_2) \cdot 0.0001]$  diagram, after Winchester and Floyd (1977). B, Zr–Ti/100– $Y \cdot 3$  diagram, after Pearce and Cann (1973). C, chondrite-normalized REE patterns for moderate-Ti and high-Ti trachydolerite.

geochemical features, but the high-Ti rock is richer in  $FeO'$ , HFSE (P, Zr, Y) and REE (Table 2). The REE patterns of both subgroups are gently dipping and almost parallel (Fig. 6C) with  $La_n/Yb_n \approx 8$  and  $Eu^*/Eu \approx 0.85$  (Table 2).

The high proportion of secondary minerals (chlorite, actinolite, sericite, carbonate, hematite) even in the least altered samples suggests that the observed contents of alkalis and other mobile elements might not correspond to the original magmatic values. Therefore classification diagrams based on immobile trace elements are used. In the Nb/Y vs Zr/TiO<sub>2</sub> diagram (Fig. 6A) compositions of both moderate-Ti and high-Ti trachydolerites plot in the field of subalka-

line basalt. In the Zr–Ti–Y geotectonic classification diagram (Fig. 6B) all data points plot in the field of within-plate basalts.

Rocks of intermediate composition forming mafic margins with abrupt contacts in composite dykes and rare simple mafic dykes plot in the field of andesite and dacite in the Nb/Y vs Zr/TiO<sub>2</sub> classification diagram (Fig. 6A). The chemical affinities of the intermediate rocks are described below, in the discussion that concerns the interaction between coeval silicic and mafic magmas.

## 6. Stable and radiogenic isotope ratios

### 6.1. Oxygen isotopes

Oxygen isotope ratios were measured in rock-forming minerals from felsic and mafic rocks (quartz, alkali feldspar, plagioclase, augite) and in zircon from the quartz porphyry (Table 4; Fig. 7). The whole-rock  $\delta^{18}O$  values that were measured in samples analyzed for radiogenic isotopes are listed in Table 5.

In a trachydolerite from a composite dyke the  $\delta^{18}O$  of clinopyroxene is 5.78‰ (Fig. 7), which is within the  $\delta^{18}O$  range of clinopyroxene in the mantle (Mattey et al., 1994a) and is similar to the  $\delta^{18}O(Cpx)$  of modern basalts from the Taupo volcanic zone (New Zealand) erupted through the continental crust (Macpherson et al., 1998). This suggests that the oxygen isotope ratio of

Table 4  
 $\delta^{18}O$  values (‰, SMOW) in minerals from dyke rocks

Sample no.	Rock	Qtz	Afs [Pl]	Zrn [Cpx]
<i>Bimodal dyke suite 3</i>				
A197-6	trachydolerite		[11.16]	[5.78]
A52	quartz porphyry, stock	9.10	11.86	6.49
A197	quartz porphyry, dyke	8.57	13.27	
A197-1	"	8.60	13.12	6.45
A-129	"	8.9		
A-157	"	8.71	14.73	
A198	"	9.69	12.95	7.23
A202	"	9.65	13.41	
A128	"	8.75	10.67	
A149	"	8.9	14.1	
A285	"	8.3	15.45	
D218a	"	8.68	13.43	
<i>Dyke suite 2</i>				
A148	andesite porphyry		[11.13]	
A160-1	dacite porphyry		[13.58]	
<i>Dyke suite 1</i>				
A173a	microdiorite		[11.12]	
A28	lamprophyre		[10.06]	
A25	"		[10.84]	

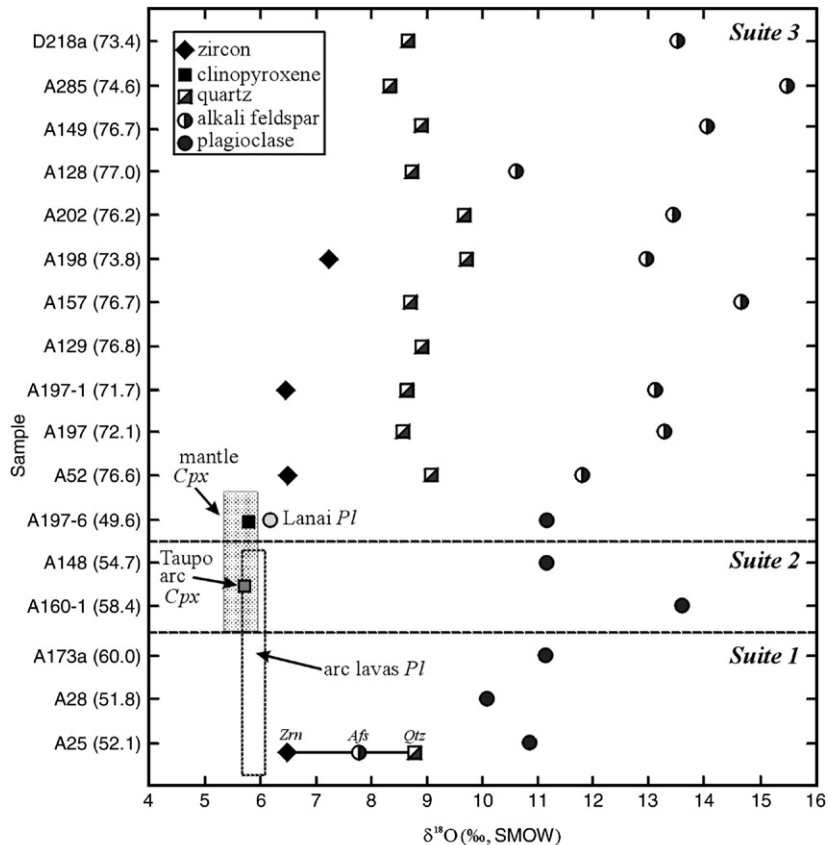


Fig. 7. Oxygen isotope ratios of mineral separates from the Late Neoproterozoic dyke suites of southern Israel. The  $\text{SiO}_2$  (wt.%) content is denoted in parentheses. The shaded band marks the range of  $\delta^{18}\text{O}$  values of clinopyroxene in mantle xenoliths (Mattey et al., 1994a,b). The dashed rectangle illustrates the  $\delta^{18}\text{O}$  range of plagioclase in oceanic arc lavas (Eiler et al., 2000). Also shown are the average  $\delta^{18}\text{O}$  values of clinopyroxene phenocrysts from basalts and andesites of the Taupo arc, New Zealand and of plagioclase from the Lanai volcano, Hawaii (Eiler et al., 1996; Macpherson et al., 1998). The Zrn–Afs–Qtz bar shows equilibrium fractionations between the minerals at magmatic temperatures (after Chiba et al., 1989; Valley et al., 2003).

clinopyroxene from the trachydolerite was not modified after the initial isotope equilibrium with the mantle source rock. Notwithstanding, plagioclase of the trachydolerite has a non-magmatic high  $\delta^{18}\text{O}$  value of about 11‰ (Fig. 7). Similar values are also characteristic of plagioclase in mafic rocks from earlier dyke suites (Fig. 7). Experimentally calibrated plagioclase–clinopyroxene isotope fractionations at temperatures of crystallization of basaltic melts (1100–1200 °C) are  $\leq 0.7\text{‰}$  (Chiba et al., 1989). Oxygen isotope ratios of plagioclase from recently erupted oceanic arc lavas range from 5.6 to 5.9‰ (Eiler et al., 2000). Likewise  $\delta^{18}\text{O}(\text{Pl})$  of historic subaerial alkaline basalt from the Lanai volcano, Hawaii is 6.08‰ (Eiler et al., 1996). Thus, the  $\delta^{18}\text{O}$  values of plagioclase in the Elat mafic dykes are 4 to 5‰ higher than their original magmatic equilibrium values.

Oxygen isotope ratios of zircon in quartz porphyry from composite dykes and from a subvolcanic stock range from 6.45 to 7.23‰. These values are significantly higher than  $\delta^{18}\text{O}$  of mantle zircon:  $5.3 \pm 0.6\text{‰}$  ( $2\sigma$ ; Valley, 2003). Since zircon is the best preserver of initial magmatic values (Valley et al., 1994; Page et al., 2006) the relatively high  $\delta^{18}\text{O}(\text{Zrn})$  of quartz porphyry suggests contribution of upper crustal sources to the rhyolite magma. This stands in contrast to the mantle  $\delta^{18}\text{O}$  of clinopyroxene from the trachydolerite and suggests variable sources for the coexisting magmas.

In 11 samples collected from different quartz porphyry dykes, the  $\delta^{18}\text{O}$  values of quartz range from 8.30 to 9.70‰ (Table 4; Fig. 7). The measured  $\Delta^{18}\text{O}$  (Qtz–Zrn), 2.15 to 2.61‰, does not differ markedly from the predicted magmatic quartz–zircon isotope fractionation, 2.3‰ at  $T=800\text{ °C}$  (Valley et al., 2003).

Table 5

Nd–Sr and  $\delta^{18}\text{O}$  (WR) isotope compositions of rocks from the dyke suite 3 (southern Israel) and the Katharina ring complex (Sinai, Egypt)

Sample no.	Rock	Rb (ppm)	Sr (ppm)	$^{87}\text{Rb}/$ $^{86}\text{Sr}$	$^{87}\text{Sr}/$ $^{86}\text{Sr}$	$\pm 2\sigma$	I (Sr)	Sm (ppm)	Nd (ppm)	$^{147}\text{Sm}/$ $^{144}\text{Nd}$	$^{143}\text{Nd}/$ $^{144}\text{Nd}$	$\pm 2\sigma$	$\epsilon_{\text{Nd}}$ (0)	$\epsilon_{\text{Nd}}$ (T)	$f$ (Sm/Nd)	$T_{\text{DM}-1}$ (Ma)	$T_{\text{DM}-2}$ (Ma)	$\delta^{18}\text{O}$ WR	
<i>Dyke suite 3 (590 Ma)</i>																			
A18	quartz porphyry	144.6	78.3	5.38	0.780104	15	0.73483	11.51	55.33	0.1258	0.512484	9	-3.0	2.3	-0.36	1154	1077	11.71	
A66-3	"	211.5	103.8	5.94	0.781755	11	0.73180	11.59	49.75	0.1408	0.512544	8	-1.8	2.4	-0.28	1267	1001	12.76	
A30	"	102.7	50.9	5.88	0.785968	14	0.73648	9.41	32.18	0.1768	0.512606	10	-0.6	0.9	-0.10			11.49	
A127	"	97.8	73.7	3.86	0.759867	16	0.72740	11.87	58.84	0.1220	0.512510	12	-2.5	3.1	-0.38	1063	1030	12.16	
A198	"	119.9	126.0	2.76	0.742676	11	0.71943	10.33	46.70	0.1337	0.512465	18	-3.4	1.4	-0.32	1304	1118	11.52	
A147-2	rhyolite porphyry	86.3	54.9	4.58	0.773803	17	0.73529	8.14	40.59	0.1212	0.512476	15	-3.2	2.5	-0.38	1111	1083	11.15	
A156-1	"	106.6	157.7	1.96	0.728985	13	0.71253	5.84	22.54	0.1566	0.512553	10	-1.7	1.4	-0.20	1591	1008	9.79	
A196-1	trachydolerite	70.0	457.1	0.44	0.708304	10	0.70458	6.64	31.82	0.1262	0.512502	10	-2.7	2.7	-0.36	1128		10.54	
N-1	"	40.7	698.7	0.17	0.707539	14	0.70612	5.63	27.68	0.1230	0.512486	14	-3.0	2.6	-0.37	1115		9.24	
D21aa	"	101.8	166.7	1.77	0.727299	12	0.71241	11.03	50.04	0.1333	0.512494	11	-2.8	2.0	-0.32	1242		10.5	
A196-4a	trachyandesite							6.73	32.73	0.1243	0.512478	12	-3.1	2.3	-0.37	1145		10.92	
A127-2	"							9.87	47.30	0.1262	0.512535	12	-2.0	3.3	-0.36	1070		13.1	
<i>Katharina ring complex (590 Ma)</i>																			
D163	syenogranite, pluton	220.5	91.29	7.01	0.758037	8	0.69904	6.34	32.57	0.1177	0.512519	3	-2.3	3.6	-0.40	1002	1010	9.18	
D165	"	238.3	86.75	7.98	0.767362	8	0.70020	7.26	36.33	0.1208	0.512546	3	-1.8	3.9	-0.39	991	971	8.15	
IL-66	quartz monz. porphyry	53.8	396.9	0.37	0.706085	7	0.70300	10.97	62.42	0.1062	0.512571	3	-1.3	5.5	-0.46	822	911	7.12	
IL-161	quartz syenite porphyry	99.6	305.3	0.94	0.710773	7	0.70284	12.08	72.82	0.1003	0.512503	3	-2.6	4.6	-0.49	870	1012	7.13	
AG-32	peralk. granite porphyry	204.9	8.96	69.85	1.291379	10	0.70372	12.17	63.49	0.1159	0.512558	3	-1.6	4.5	-0.41	923	945	9.19	

(1) To obtain meaningful model ages,  $T_{\text{DM}}$  were calculated for samples with  $f(\text{Sm}/\text{Nd})$  that range from -0.2 to -0.6 (Wu et al., 2002).(2) For mafic rocks only one-stage model age ( $T_{\text{DM}-1}$ ) was calculated.

(3) Samples IL-66, IL-161 and AG-32 are from ring dykes.

This attests that in most dykes quartz was subjected to only minor modification of the magmatic  $\delta^{18}\text{O}$  during post-crystallization cooling.

In contrast to the rather limited variation in oxygen isotope ratios of quartz ( $\sim 1.4\%$ ,  $n = 10$ ), the  $\delta^{18}\text{O}$  values of alkali feldspar range from 10.67 to 15.45‰. The  $\delta^{18}\text{O}$  (Qtz–Afs) values are always negative (reversed) and range mostly from  $-4$  to  $-6\%$  (Table 5; Fig. 13), which is far from the experimentally determined magmatic equilibrium fractionation of  $+1\%$  at  $700\text{ }^\circ\text{C}$  (Clayton et al., 1989). Thus, the  $\delta^{18}\text{O}$  values for alkali feldspar in quartz porphyry were extremely elevated by a post-magmatic process.

Whole-rock samples from felsic and mafic rocks (Table 5) are characterized by high  $\delta^{18}\text{O}$  values, commonly  $>10\%$ , mostly affected by the elevated  $\delta^{18}\text{O}$  values of feldspars, which are the most modally abundant phase in both groups and most readily exchange oxygen during sub-solidus alteration. The whole-rock oxygen isotope data are discussed in the next section.

## 6.2. Radiogenic isotope ratios

Rb–Sr and Sm–Nd data for 12 whole-rock samples including silicic and mafic dyke rocks are given in Table 5. For comparison, isotope data for the Katharina ring complex (southern Sinai), which is made up of Late Pan-African A-type granite and related ring dyke rocks (Eyal and Hezkiyahu, 1980; Katzir et al., 2007), are also presented in Table 5.

The calculated initial  $^{87}\text{Sr}/^{86}\text{Sr}$  ratios ( $=I(\text{Sr})$  at 590 Ma) range from ca. 0.704 (trachydolerite A196-1) to ca. 0.737 (quartz porphyry, A-30). The  $I(\text{Sr})$  values in felsic rocks are not only high, but also extremely variable, ranging from 0.71253 to 0.73648 (Table 5), which precludes calculation of an isochron and suggests postmagmatic disturbance of the Rb–Sr system.

The Sm–Nd isotopic data seem to provide much more coherent information about the petrogenesis of the dyke rocks. The initial  $^{143}\text{Nd}/^{144}\text{Nd}$  ratios, expressed as  $\varepsilon_{\text{Nd}}(T)$  values do not correlate with the initial Sr values (Fig. 8). They are fairly uniform and range from  $+0.9$  to  $+3.3$ . Given the analytical error of  $\pm 0.5$   $\varepsilon$ -unit, there is no systematic and significant difference between  $\varepsilon_{\text{Nd}}(T)$  values of felsic and mafic dyke rocks. However, the range of  $\varepsilon_{\text{Nd}}(T)$  values is clearly lower than that of the Katharina Complex ( $+3.6$  to  $+5.5$ ). The difference is also reflected by the oxygen isotope data (see Table 5, last column) to be presented below. The Sm–Nd model ages, calculated for felsic rocks with a two-stage model, range from ca. 1000 to 1100 Ma. This range is rather

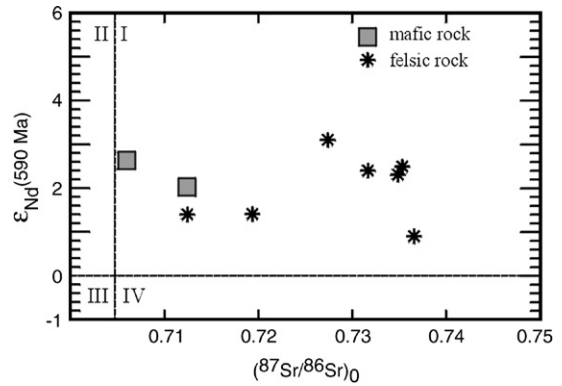


Fig. 8.  $\varepsilon_{\text{Nd}}(590\text{ Ma})$  vs  $(^{87}\text{Sr}/^{86}\text{Sr})_0$  in dykes from the bimodal suite. Note the narrow range of  $\varepsilon_{\text{Nd}}(T)$  values in mafic and felsic rocks irrespective of  $(^{87}\text{Sr}/^{86}\text{Sr})_0$  values.

similar to that of the Katharina Complex. Comparatively young model ages are characteristic of most Precambrian rocks throughout the Arabian–Nubian shield supporting the idea of juvenile Neoproterozoic continental crust in the shield (Stein and Goldstein, 1996).

## 7. Discussion

### 7.1. Effect of alteration on the original chemical composition of the dyke rocks

The abundance of secondary minerals and the significant elevation of the oxygen isotope ratios of feldspar even in the seemingly least altered felsic and mafic rocks indicate that the dyke rocks were subjected to rather extensive alteration. Also the calculated whole-rock  $(^{87}\text{Sr}/^{86}\text{Sr})_0$  values for 590 Ma in quartz porphyry and rhyolite porphyry are unusually high and vary over a wide range. The Rb–Sr isotope data do not allow calculating an isochron. This raises the question of how well the original chemical composition of the dyke rocks has been preserved under conditions of postmagmatic alteration. We approached this problem by comparing quartz porphyry and trachydolerite from southern Israel to similar rock types from adjacent regions, the Northeastern Desert, Egypt and southwestern Jordan. According to Stern et al. (1988) and Jarrar et al. (2004), these rocks have been subjected to rather mild alteration that did not prevent dating them by the Rb–Sr method. Unfortunately, there is not a single key area in which both felsic and mafic rocks can be used for comparison as reference rocks. In particular, in southwestern Jordan the rhyolite from composite dykes is chemically uniform and contains 75–77 wt.%  $\text{SiO}_2$ , but mafic margins are made up of hybrid latite

(Jarrar et al., 2004). In the Northeastern Desert dolerite is abundant in the bimodal dyke swarm, whereas rhyolite is characterized by wide range of  $\text{SiO}_2$ , from 69 wt.% to 77 wt.%, and the origin of low- $\text{SiO}_2$  rhyolite is debatable (Stern et al., 1988). For this reason we have chosen the dolerite from the Northeastern Desert and rhyolite from southwestern Jordan as reference rocks for normalization. A comparison of normalized average volatile-free compositions of felsic rocks with  $\geq 75$  wt.%  $\text{SiO}_2$  and mafic rocks with 49–56 wt.%  $\text{SiO}_2$  (Table 2; supplementary data, Table 4S) is presented by spidergrams (Fig. 9).

The patterns in Fig. 9A show that within one standard deviation the felsic rocks from all three regions are fairly similar in Th, Y, La, Sm, Gd and in the mobile LIL element contents (Rb, K, and Na). Rhyolites from southern Israel and the Northeastern Desert, as compared to felsic rocks from southwestern Jordan, are richer in Nb, Zr, Ce, Yb and poorer in Sr. This points to their more alkaline character and suggests that the observed chemical distinctions are caused by original compositional features of the silicic magmas in the

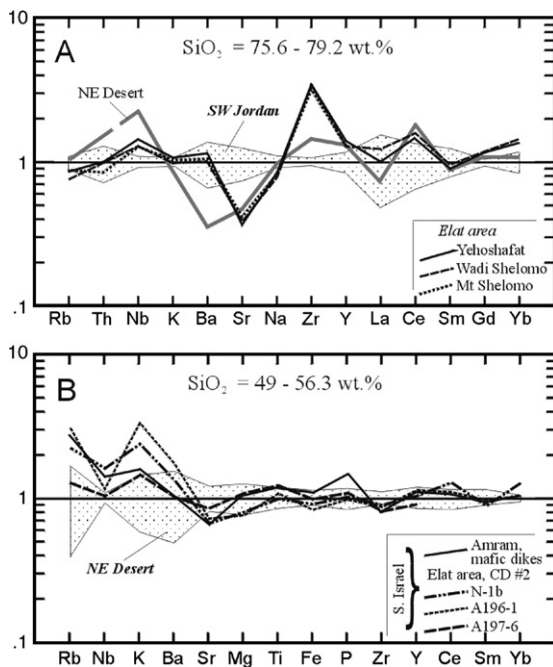


Fig. 9. Spidergrams of felsic (A) and mafic (B) rocks from the bimodal dyke suite in southern Israel normalized to well-preserved Late Neoproterozoic dyke rocks from similar suites in Egypt and Jordan (see text for more details). A, normalized to rhyolite from southwestern Jordan (Jarrar et al., 2004); B, normalized to dolerite from the Northeastern Desert, Egypt (Stern et al., 1988). Stippled areas are  $\pm 1\sigma$  range of rock compositions used for normalization. A full set of data is given in Table 3S of the supplementary data.

different regions rather than by migration of elements in the process of alteration. It is thus concluded that the initial igneous composition of the felsic dyke rocks is sufficiently well preserved.

Chemical data for mafic rocks are compared in Fig. 9B. The plot shows that the chemical compositions of trachydolerite from southern Israel and of mafic rocks from the bimodal dyke suite in Egypt are essentially similar. The main distinction is the higher K and Rb contents of the S. Israel rocks. It is conceivable that the K and Rb enrichment was partly caused by metasomatic alteration (Agron and Bentor, 1981; Wachendorf et al., 1985). The original concentration of these elements cannot be quantitatively assessed. We assume that it is comparable to that of the mafic dykes from the Northeastern Desert, namely about 2 wt.%  $\text{K}_2\text{O}$  and  $\sim 50$  ppm Rb.

### 7.2. Interaction of mafic and silicic magma

Field, petrographic and chemical data indicate that interaction between mafic and silicic magmas occurred during the formation of the bimodal dyke suite. Interaction occurred both in situ, in the process of composite dyke formation, and at greater depth from which hybrid magmas were injected to the subsurface level.

The most graphic example of in situ interaction between rhyolite and basalt magmas is the Netafim dyke #2 (Fig. 10). Symmetric structure and gradational contacts between felsic interior and mafic margins show that the injection of silicic magma occurred when part of the basic melt had not yet solidified. The phenocryst assemblages in the trachydacite and trachyandesite from the transitional zone were derived from both end-member magmas. This points to mutual penetration of two adjacent partially crystallized magmas that already contained phenocrysts.

Variation of rock chemistry across dyke #2 is shown in Table 3 and in a set of diagrams (Fig. 10). Both major and selected trace elements (except Ba) demonstrate symmetrical and regular change from quartz porphyry through the hybrid trachydacite and trachyandesite to trachydolerite. The only noticeable discrepancy in the distribution of  $\text{Na}_2\text{O}$ ,  $\text{K}_2\text{O}$ , and Rb is seen in one sample from quartz porphyry (sample 8) that contains small mafic schlieren. Progressing from quartz porphyry to trachydolerite, REE contents decrease and  $\text{Eu}/\text{Eu}^*$  increases systematically as expected in mixing of silicic and mafic end members (Fig. 11).

In a series of silica variation diagrams (Fig. 12) the data points are mostly arranged along straight regression lines connecting end-members, with R-values close to unity.

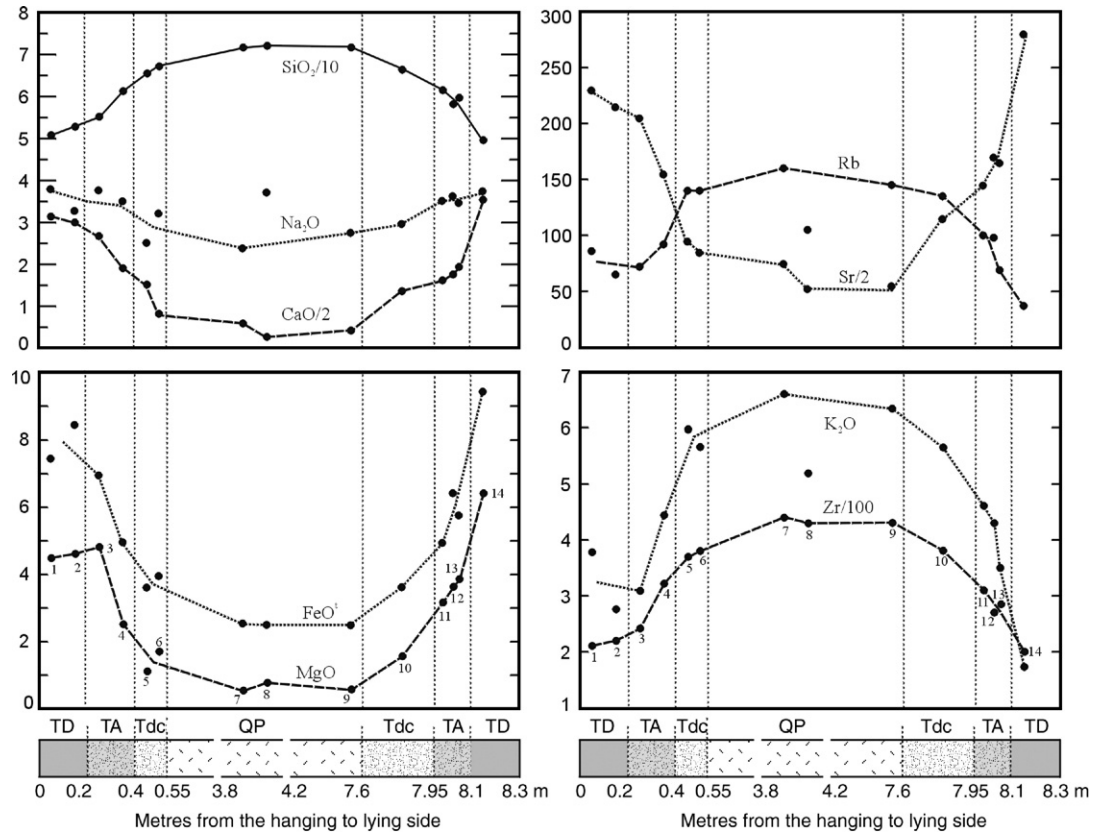


Fig. 10. Compositional profiles across the Netafim composite dyke #2 (plots of selected major and trace elements versus distance). Zones within the dyke: TD = trachydolerite; mixing zone: TA = hybrid trachyandesite, Tdc = hybrid trachydacite; QP = quartz porphyry. Sample numbers are the same as in Table 3. Major elements, wt.%; trace elements, ppm.

The scattering in the Ba and Rb data possibly stems from fast chemical diffusion superimposed on bulk mixing. Thus, chemical data are in a good consistency with structural and petrographic evidence indicating that the

main process responsible for the formation of the hybrid rocks in the composite dyke #2 was magma mixing.

Mass balance calculations performed for major and trace elements show that the trachyandesite could form by mixing of the basalt and rhyolite components in proportions of 57% and 43% respectively, whereas for trachydacite the proportions are 20.5% and 79.5%, respectively (Table 6, calculated using program Igpet for Windows, 1994).

Composite dykes with gradational contacts like composite dyke #2 are not common in the Elat area. Actually, dykes with abrupt contacts are dominant and in many of them the mafic margins are made up of trachyandesite and trachydacite. In places these rocks make up simple dykes. The intermediate rocks are often heterogeneous and contain xenocrysts of quartz, K-feldspar and plagioclase with sieve-like texture. These features show that magma mixing was important in the genesis of the intermediate rocks. Abrupt contacts in composite dykes attest that hybrid magmas were produced mainly at greater depth prior to emplacement.

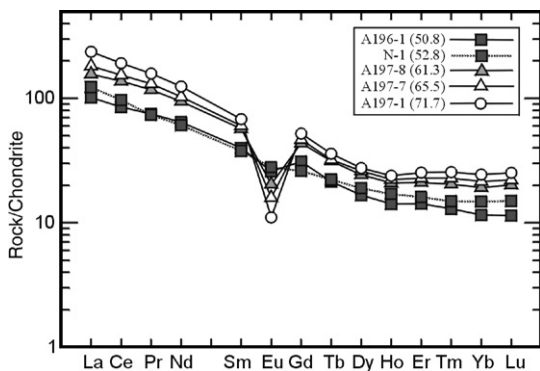


Fig. 11. Chondrite-normalized REE patterns for rocks from the Netafim composite dyke #2. The pattern numbers correspond to the sample numbers in Table 3; in parentheses: silica content (wt.%).

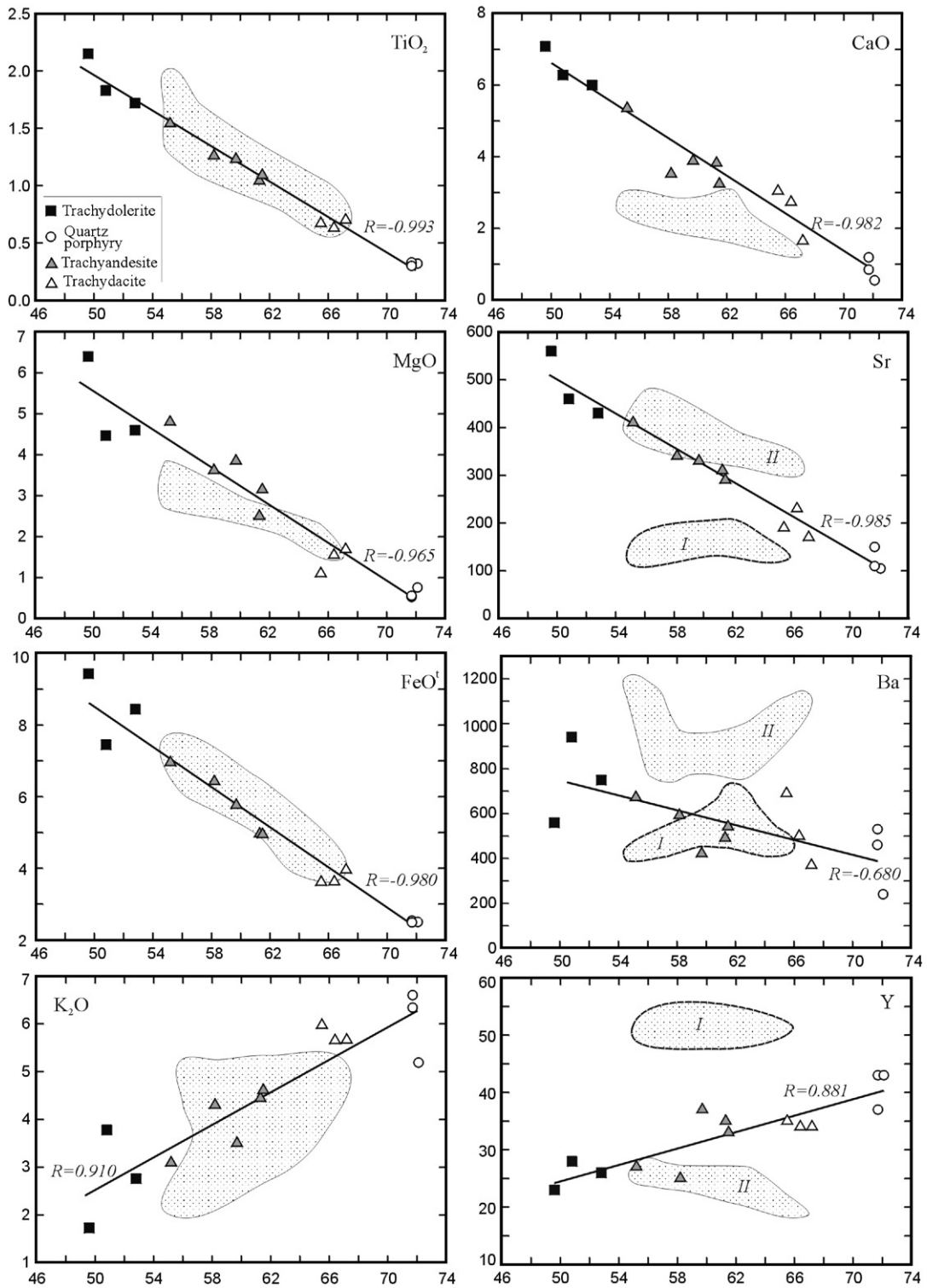


Fig. 12. Silica variation diagrams for rocks making up the Netafim composite dyke #2 with regression lines and the correlation coefficient values (R). Stippled fields denote compositions of intermediate rocks from composite dykes with abrupt contacts, and simple andesite dykes; I and II, groups of dyke rocks (see text).

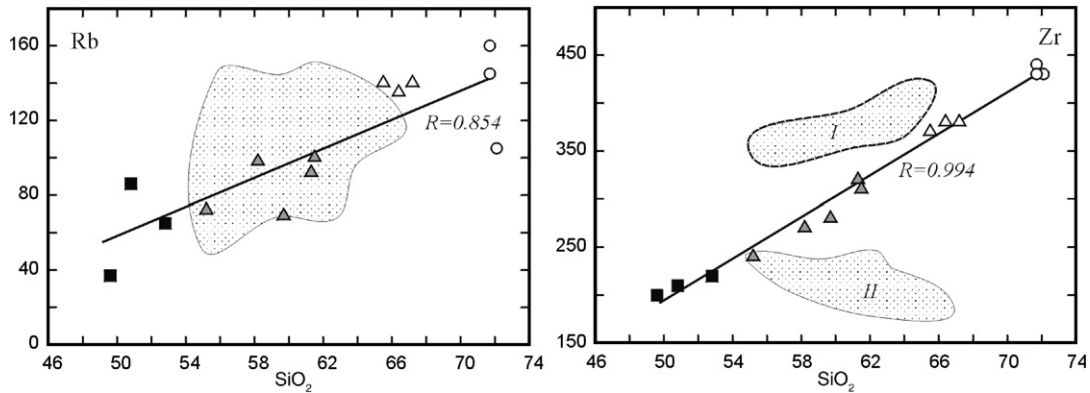


Fig. 12 (continued).

Chemical compositions of intermediate rocks are plotted in binary diagrams (Fig. 12) and show rather restricted similarity with the in situ produced hybrid rocks from the Netafim dyke. Only less mobile major elements tend to be arranged close to the mixing lines. Elements with high diffusivity,  $K_2O$  and Rb, demonstrate large scatter, which points to the great role of diffusive exchange between co-existing magmas (Zorpi et al., 1991; Poli and Tommazini, 1991; Litvinovsky et al., 1995b). The distinctions in other trace elements are more significant. Intermediate rocks are clearly divided into two groups with different Sr, Ba, Zr, Nb, and Y concentrations, and neither of them is similar to the in situ formed hybrid rocks (Fig. 12, Tables 1 and 2; Table 3S, supplementary data). It is likely that magma mixing processes had not been frozen at the initial stage as it occurred in the Netafim dyke. At greater depth mixing could have progressed to much higher extent and may have been followed by fractional crystallization and assimilation. Some variations in the end-member compositions are also possible.

### 7.3. Oxygen isotope evidence of late alteration of dyke rocks

Initial magmatic  $^{18}O/^{16}O$  ratios have been retained only in two minerals from the dyke rocks: zircon in felsic rocks and clinopyroxene in trachydolerite. The relatively small variation in  $\delta^{18}O(Qtz)$  and the magmatic-like  $\Delta^{18}O(Qtz-Zrn)$  in the dykes indicate that the oxygen isotope ratio of quartz was only slightly modified after crystallization (Fig. 7). However, the magmatic  $\delta^{18}O$  values of feldspars were significantly altered. Isotope ratios of quartz and alkali-feldspar from quartz porphyry dykes are presented in a  $\delta$ - $\delta$  diagram (Fig. 13). For comparison, isotope data on alkaline

granites from southern Israel and Sinai Peninsula (the Katharina ring complex) are also shown (the data are compiled in Table 7). The  $\delta^{18}O$  values for quartz in each rock unit is almost uniform, while  $\delta^{18}O(Afs)$  is highly variable thus forming well-defined, narrow and vertically elongated arrays in the plot. A notable difference between granites and dykes is clearly exhibited:  $\Delta^{18}O(Qtz-Afs)$  in quartz porphyries are always negative and range mostly from  $-2$  to  $-6\text{‰}$ , whereas in the granites these values vary from  $-0.7$  to  $-2.0\text{‰}$ . Measured quartz-alkali feldspar isotope fractionations in fresh granites worldwide are typically about  $+1$  to  $+1.5\text{‰}$  (Criss and Taylor, 1983). These are slightly larger than the experimentally determined equilibrium  $\Delta^{18}O(Qtz-Ab)$  at  $800\text{ °C}$  ( $0.8\text{‰}$ ; Clayton et al., 1989) and probably reflect inter-mineral subsolidus oxygen exchange during cooling. It follows that the magmatic  $^{18}O/^{16}O$  ratio of feldspar was elevated by exchange with external reservoir both in plutonic and dyke rocks, but in the latter the elevation was extreme (up to  $8\text{‰}$ ).

Quartz is much more resistant than feldspar to hydrothermal  $^{18}O/^{16}O$  exchange. The preservation of magmatic  $\delta^{18}O$  values in quartz on the one hand and the marked increase in  $\delta^{18}O(Afs)$  on the other hand indicate that dykes experienced intense water-rock interaction. However, high-temperature ( $250$ – $500\text{ °C}$ ) hydrothermal alteration by circulating meteoric water heated by a cooling pluton, which is indicated in many shallow intrusions (e.g., Criss and Taylor, 1983), can be ruled out. Oxygen exchange with hot meteoric water would instead appreciably decrease the isotopic ratio of feldspar relative to quartz to form highly positive quartz-alkali feldspar fractionations (Criss and Taylor, 1983, 1986). A simple closed-system, water-rock exchange model indicates that the observed high  $\delta^{18}O$  values of feldspar in the felsic dykes ( $+11$  to  $+16\text{‰}$ )

Table 6  
Results of modelling of magma mixing for the Netafim composite dyke #2

Sample wt.%	Mixing magmas		Hybrid magmas			
	Trachydolerite	Qtz porphyry	Trachyandesite (n=5)		Trachydacite (n=3)	
	n=3	n=3	Observed	Calculated	Observed	Calculated
SiO <sub>2</sub>	54.28	73.15	61.79	62.07	68.69	68.99
TiO <sub>2</sub>	2.02	0.33	1.28	1.28	0.69	0.67
Al <sub>2</sub> O <sub>3</sub>	16.15	13.24	14.83	14.81	13.63	13.78
FeO <sup>t</sup>	8.97	2.56	6.07	6.16	3.85	3.86
MgO	5.48	0.63	3.74	3.36	1.50	1.62
CaO	6.85	0.88	4.14	4.25	2.55	2.09
Na <sub>2</sub> O	3.83	3	3.73	3.45	2.99	3.16
K <sub>2</sub> O	[2.00]	6.15	4.17	3.77	5.96	5.28
P <sub>2</sub> O <sub>5</sub>	0.42	0.05	0.26	0.26	0.13	0.13
Sum residuals squared				0.40		0.74
<i>Mixing components (wt.%)</i>						
Basic magma				56.8		20.5
Felsic magma				43.2		79.5
ppm						
Rb	[50]	137	86	87	138	118
Ba	750	410	543	600	520	478
Sr	483	122	336	326	197	195
Zr	210	433	285	305	377	386
Nb	14	29	19	21	25	26
Y	26	41	32	32	34	38
La	26	56	37	39	43	50
Ce	55	117	84	81	94	104
Nd	29	58	44	41	48	52
Sm	5.9	10.4	8.7	7.8	9.2	9.4
Eu	1.54	0.64	1.18	1.1	0.92	0.8
Gd	5.8	10.7	9	8	9.6	9.7
Dy	4.5	7	6.2	5.5	6.6	6.4
Er	2.48	4.18	3.48	3.2	3.77	3.89
Yb	2.21	4.15	3.26	3	3.65	3.7

(1) Modelling was done using the program IGPET (Terra Softa Inc., 1994).

(2) In rock compositions major elements are recalculated to total = 100% volatile free.

(3) In trachydolerite, accepted contents of K<sub>2</sub>O=2 wt.% and Rb=50 ppm are in brackets (see Section 7.1).

(4) Total Fe as FeO<sup>t</sup>.

require very low temperatures of alteration ( $\leq 100$  °C), if it occurred by exchange with typical meteoric water of  $\delta^{18}\text{O}(\text{H}_2\text{O}) = -5$  to  $-15\%$  (Wenner and Taylor, 1976).

Low-temperature alteration of quartz porphyry is also indicated by extensive reddening and turbidization of alkali feldspar. Likewise, plagioclase in the mafic dykes is commonly sericitized, turbid and characterized by significant loss of Ca, culminating in almost complete albitization of labradorite–andesine (Litvinovsky et al., in press). Therefore the 4 to 5‰ elevation of  $\delta^{18}\text{O}$  (Pl) relative to its inferred magmatic ratios (Fig. 7) could also have occurred by low-temperature interaction with meteoric water. Alternatively, higher temperature alteration should involve unusually  $^{18}\text{O}/^{16}\text{O}$ -rich waters. High temperature ( $\sim 250$  °C) interaction with high- $\delta^{18}\text{O}$  brines (+3‰) was suggested to account for the

moderately negative  $\Delta^{18}\text{O}$  (Qtz–Pl) ( $-1$  to  $-1.4\%$ ) measured in Timna mafic and felsic plutonic rocks (Beyth et al., 1997). The hydrothermal activity presumably responsible for the  $^{18}\text{O}/^{16}\text{O}$  enrichments in the Timna igneous complex was attributed to circulation of brines through fractures related to the Dead Sea transform (Beyth et al., 1997; Matthews et al., 1999). The alleged timing of the hydrothermal event was largely based on the chemical remanent magnetization of Miocene age measured in the Timna igneous rocks (Marco et al., 1993). Here we show that postmagmatic  $^{18}\text{O}/^{16}\text{O}$  elevations in feldspars, and consequently in whole rocks, are not restricted to the Timna area, but characterize dykes and plutons throughout the order of magnitude larger Elat area. Moreover, Late Neoproterozoic alkaline granite, the Katharina pluton, that

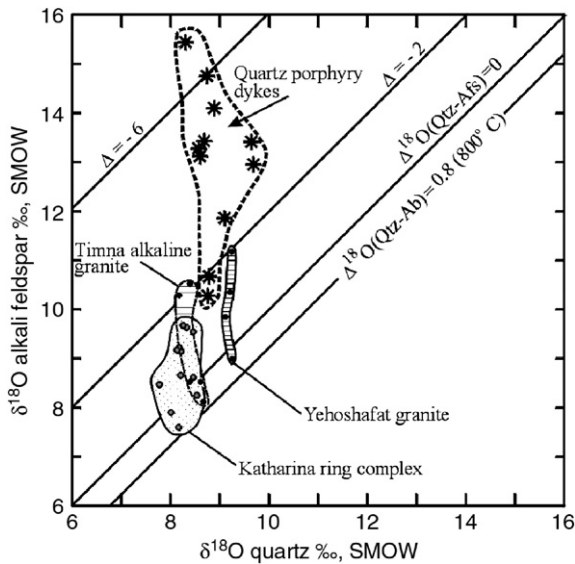


Fig. 13.  $\delta$ – $\delta$  diagrams for quartz and alkali feldspar in quartz porphyry from the bimodal suite (asterisks). Isotherm for equilibrium fractionation between Qtz and Ab at 800 °C is after Clayton et al. (1989). For comparison, data for three Late Neoproterozoic granite complexes are presented (see text).

outcrops > 50 km away from the Dead Sea transform in central southern Sinai also shows mild  $^{18}\text{O}/^{16}\text{O}$ -enrichments in its uppermost part that is comparable to those measured in Timna. The origin(s) and timing(s) of the elevation of isotope ratios that is characteristic of a large area in the northernmost ANS are yet to be determined. Our results show, however, that late oxygen exchange with external fluids occurred not only in the bimodal dyke suite, but also in dykes from the two preceding suites (Fig. 7; Table 4). This attests that the alteration process was not linked with injection of a specific batch of magma. Presumably the extensive water–rock exchange happened mainly in dykes since dyke injections are commonly controlled or followed by fault zones that accommodate circulation of water. Less intense  $^{18}\text{O}/^{16}\text{O}$  variations in the host granites (Fig. 13) may be explained by the fact that these rocks were sampled at sites with no evidence of fracturing and rock alteration.

#### 7.4. Origin of the unusual I(Sr) values in the quartz porphyry dykes

The I(Sr) (590 Ma) values for individual quartz and rhyolite porphyry dykes from the bimodal suite vary widely, from 0.71253 to 0.73648 (Table 5), and the Rb–Sr isotope data do not allow calculation of a realistic isochron. In a classic diagram of I(Sr) vs  $\varepsilon_{\text{Nd}}(T)$  (Fig. 8),

the data points of the dyke rocks fall in the first quadrangle, which is totally unexpected from felsic igneous rocks. This indicates a pronounced disturbance of the pristine Rb–Sr isotope system that could have occurred either at the magmatic or post-crystallization stage.

Table 7

$\delta^{18}\text{O}$  values (‰, SMOW) in minerals from plutonic and metamorphic rocks from southern Israel and the Katharina ring complex, Sinai

Sample no.	Rock	Qtz	Afs [PI]	Zrn
<i>Elat granitic gneiss, 740 Ma (Eyal et al., 1991)*</i>				
YE-8		11.81	10.79	6.67
YE-9		9.97	9.45	7.09
YE-16		11.44	10.54	6.68
YE-24		10.19	9.91	7.23
<i>Calc-alkaline Elat granite, 620 Ma (Eyal et al., 2004)</i>				
YE-11	Monzogranite	10.38	10.51	7.15
YE-33	"	10.31	9.42	6.97
YE-34	"	10.71	10.06	6.36
YE-30	"	11.17	9.83	
<i>Alkaline Yehoshafat granite, 605 ± 4 Ma (unpublished authors' data)</i>				
YE-36	syenogranite	9.26	11.18	6.76
YE-10	"	9.27	9.00	
YE-35	"	9.22	10.35	6.52
AG-81	"	9.13	9.85	6.6
<i>Timna complex, southern Israel, ~610 Ma (Beyth et al., 1994)</i>				
AG-40	Quartz syenite		8.95 [7.72]	5.75
AG-62	"		8.68 [7.94]	5.82
AG-42	Alkali–feldspar granite	8.17	10.28	
AG-63	"	8.5	8.52	5.5
AG-63a	"			5.55
AG-67	"	8.67	8.11	5.48
AG-68	"	8.4	10.53	
<i>Katharina ring complex, Sinai Peninsula, ~590 Ma (Katzir et al., 2007)</i>				
D111	Syenogranite, pluton	8.48	8.75	
D112	"	8.03	7.89 [7.86]	
D130	"	8.55	8.33 [7.58]	
D156	"	8.18	7.59 [7.75]	
Avg (n=6)	"			5.82 ± 0.06
D100	Ab–Afs granite, pluton	8.47	9.54 [8.31]	
D59	"	8.34	9.64 [9.12]	
D79	"	8.21	9.14	
D45	Perthite granite, pluton	8.17	9.19	
D46	"	8.27	9.66	
D48	"	8.15	9.17	
IL-8	Perthite quartz syenite–	8.22	8.65	5.48
IL-84	–porphyry, ring dyke	7.79	8.35	5.66
IL-112	"		7.87	
IL-147	"		7.91	5.49
IL-9	"		8.32	5.50

(1) \* = here and below in the table, sources for age data are given.

(2)  $\delta^{18}\text{O}$  values from Yehoshafat and Timna rocks after Gal, 2006.

(3) Avg (n=6) = composite separate of zircon from 6 samples.

At the *magmatic stage*, such a disturbance could have been caused by active interaction between coeval silicic and mafic magmas. Some experimental studies have observed that isotopic gradients homogenize roughly ten times faster than their respective chemical gradients, so a basaltic magma may thereby impart its isotopic characteristics to a silicic magma long before the chemical composition of the latter is noticeably changed (Baker, 1989, 1990; Lasher, 1990, 1994; Snyder and Tait, 1998). Also it was shown that the  $^{87}\text{Sr}/^{86}\text{Sr}$  of silicic magmas is very sensitive to input from basaltic injections, but the Nd-isotope ratios are preserved (Snyder and Tait, 1998).

Applying the isotope exchange model to the bimodal dykes of Elat, we assume that the mafic end-member had  $I(\text{Sr})$  of about 0.7050 and  $\varepsilon_{\text{Nd}}(T)=2$ , whereas the felsic end-member, i.e. the least hybridized silicic magma, had  $I(\text{Sr}) \sim 0.7400$  and  $\varepsilon_{\text{Nd}}(T) \sim 2$  (Table 5). Such isotope characteristics of the supposed silicic end-member are unusual. On the one hand, very high  $I(\text{Sr})$  value points to typical ancient continental crust source; on the other hand, the  $\varepsilon_{\text{Nd}}(T)$  values are characteristic of mildly depleted mantle or of juvenile crust. However, the main argument that testifies against isotope exchange during magma mixing is the absence of felsic rocks with high  $I(\text{Sr})$  values in the territory of the ANS. All granites and gneisses that may be regarded as possible silicic end-member sources have  $I(\text{Sr})$  values of  $<0.710$ – $0.715$ , which are characteristic of crust in juvenile provinces like the ANS (Stein and Goldstein, 1996; Stein, 2003).

In order to assess the role of *post-crystallization processes* in disturbing the Rb–Sr system, one has to acknowledge the crucial effect of alkali feldspar, the major carrier of both Rb and Sr in the felsic dykes from the bimodal suite. The water–rock interaction that resulted in the elevation of  $\delta^{18}\text{O}(\text{Afs})$  up to 13–15‰ could also cause the significant disturbance of the Rb–Sr isotope system. Indeed, a fairly clear positive correlation between  $(^{87}\text{Sr}/^{86}\text{Sr})_0$  and  $\delta^{18}\text{O}(\text{WR})$  in rhyolitic rocks is demonstrated in Fig. 14A. By contrast, in the Katharina ring complex disturbance of the initial oxygen isotope is minimal (Fig. 13), and the  $(^{87}\text{Sr}/^{86}\text{Sr})_0$  values do not correlate with  $\delta^{18}\text{O}(\text{WR})$  values (Fig. 14A), though anomalously low  $I(\text{Sr}) < 0.700$  in one sample (Table 5) indicates that the Rb–Sr isotope system did not remain fully closed. However, a Rb–Sr isochron for the Katharina complex yields an age of  $593 \pm 16$  Ma that is consistent with a U–Pb single zircon age of  $583 \pm 5$  Ma (Katzir et al., 2007), whereas for the quartz porphyry dykes a Rb–Sr age could not be calculated.

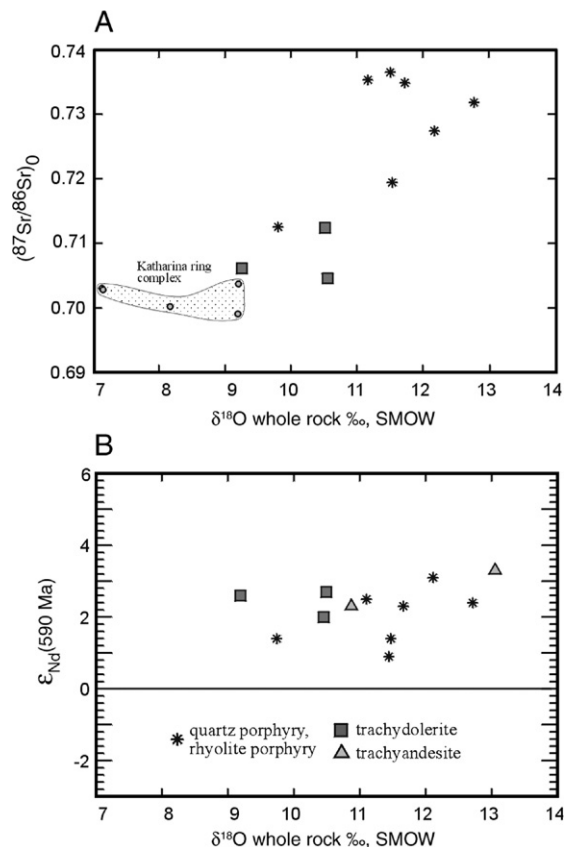


Fig. 14. Oxygen, Sr and Nd isotope ratios in mafic and felsic rocks from the bimodal dyke suite: (A) positive correlation between whole rock  $\delta^{18}\text{O}$  and  $^{87}\text{Sr}/^{86}\text{Sr}$  (590 Ma); (B) no correlation between whole rock  $\delta^{18}\text{O}$  and  $\varepsilon_{\text{Nd}}(590 \text{ Ma})$ .

In the trachydolerite increase of  $I(\text{Sr})$  values is exhibited less clearly, though the highest measured value is 0.71241 (Table 5). In mafic rocks Rb is concentrated in subordinate alkali feldspar while the main carrier of Sr is plagioclase constituting about 60% of the rock volume. Since Sr dominates over Rb, alteration of alkali feldspar that may result in resetting of its  $^{87}\text{Rb}/^{86}\text{Sr}$  and  $^{87}\text{Sr}/^{86}\text{Sr}$  ratios would not make a great impact on the whole-rock  $^{87}\text{Sr}/^{86}\text{Sr}$  value.

Thus the available radiogenic isotope data showed that the Rb–Sr isotope characteristics of the dyke rocks are dominated by late post-crystallization alteration, hence they cannot be used as petrogenetic indicators.

Low-temperature alteration that caused disturbance of the isotope systems is still poorly studied in southern Israel. Its effect on the rock chemical composition was not yet investigated in detail. However, it was shown above (Section 7.1) that the composition of felsic dyke rocks was not markedly changed by alteration processes, though in trachydolerite minor increase of  $\text{K}_2\text{O}$  and Rb contents should be considered.

### 7.5. Origin of rhyolite magmas in the bimodal dyke suite

Radiogenic and stable isotope ratios are commonly considered as the most reliable tracers of provenance of magmas. However, in the foregoing sections it was demonstrated that in the Elat area late post-crystallization processes have extensively altered the magmatic Sr isotope compositions. Unlike Sr isotope ratios,  $\epsilon_{\text{Nd}}(T)$  values of the bimodal suite vary within fairly narrow limits, from about +1.4 to +3.3 both in felsic and mafic dyke rocks and show no evidence of correlation with the whole-rock  $(^{87}\text{Sr}/^{86}\text{Sr})_0$  and  $\delta^{18}\text{O}$  values (Figs. 8 and 14B). Thus, the alteration processes have not significantly affected the Sm–Nd isotope system.

The positive  $\epsilon_{\text{Nd}}(T)$  values of the mafic dyke rocks, +2.0 to +3.3 (Table 5) indicate derivation from a mildly ‘enriched’ mantle source, similar to those associated with present day ocean island basalts (DePaolo, 1988; Stein and Goldstein, 1996). This source was more enriched relative to the ‘plume mantle’ that formed at the early stages of the evolution of the ANS and was transformed into juvenile crust and lithospheric mantle during the time interval of ~870–650 Ma (Stein, 2003). According to Stein (2003), the  $\epsilon_{\text{Nd}}$  value of the ‘plume mantle’,  $+5 \pm 1$ , did not change much during a long period, from 800 Ma to 200 Ma, owing to its low Sm/Nd ratio.

In the felsic dyke rocks the  $\epsilon_{\text{Nd}}(T)$  values vary from +0.9 to +3.1. It is likely that in places the Nd isotope system was slightly affected by alteration. For example,  $\epsilon_{\text{Nd}}(T)$  values of three samples collected from a single quartz–porphyry dyke (Fig. 1, dyke #8) are +2.3, +2.4, and +0.9 (Table 5, samples A18, A66-3, and A30). This suggests that the lowest value may be altered, thus limiting the igneous  $\epsilon_{\text{Nd}}(T)$  values of felsic rocks to the range of +1.4 to +3.1.

Apparently, the complete overlap of Nd isotope ratios in the coexisting mafic and silicic magmas can be interpreted in terms of consanguinity of mafic and silicic melts. However, in the ANS this is not the only possible interpretation since most of the crust is juvenile and relatively young (<1 Ga) and thus by the end of the Neoproterozoic it had not yet developed the radiogenic isotope signatures characteristic of ancient continental crust (Stein and Hoffman, 1992; Stern and Kröner, 1993; Furnes et al., 1996; Stein and Goldstein, 1996; Stern and Abdelsalam, 1998; Stern, 2002; Mushkin et al., 2003). In particular, it can be seen in the  $\epsilon_{\text{Nd}}(T)$  vs age diagram (Fig. 15) that two sources of alkaline rhyolite dykes are equally credible in southern Israel. The first one is coeval mafic magma evolved by fractional crystallization to form rhyolite. The second

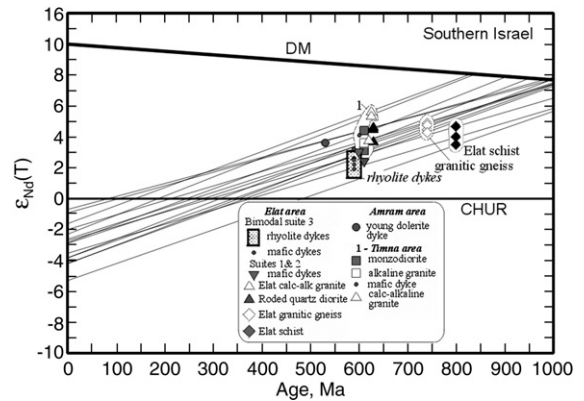


Fig. 15.  $\epsilon_{\text{Nd}}(T)$  vs age for Neoproterozoic igneous rocks and selected metamorphic rocks of southern Israel. Sources of data: Elat area, this paper (Table 5), unpublished authors’ data for Elat granitic gneiss, and Stein and Goldstein (1996); Amram area, Mushkin et al. (2003); Timna area, Beyth et al. (1994).

viable source is older metamorphic basement (granitic gneiss, crystalline schist, as well as igneous mafic rocks), which suggests formation of the rhyolite magma by partial melting of crustal material.

Regardless of the juvenile character of the crust, oxygen isotopes are a sensitive tracer of upper crustal contribution to magmas (King et al., 1998; Peck et al., 2000; Cavosie et al., 2005; Valley et al., 2005). Oxygen isotope ratios of refractory minerals reveal significant difference between the mafic and felsic dykes. Whereas clinopyroxene from the trachydolerite is characterized by a typical mantle  $\delta^{18}\text{O}$  value of 5.8‰, quartz porphyry from the same composite dyke (dyke #2) contains zircon with  $\delta^{18}\text{O}=6.45\text{‰}$ , which appreciably differs from mantle zircon values,  $5.3 \pm 0.6\text{‰}$  (2 $\sigma$ ; Valley, 2003). Other quartz porphyries from the bimodal suite have either similar (6.5‰) or higher (7.2‰) non-mantle  $\delta^{18}\text{O}(\text{Zrn})$  values (Fig. 7; Table 4). It follows that the coexisting mafic and silicic magmas of the bimodal suite differ by origin: trachydolerite evolved from mantle-derived melts, while quartz porphyry had a significant crustal component in its source.

A-type silicic magma occurs within the bimodal dyke suite in southern Israel, southwestern Jordan and Sinai, Egypt. Previous models for the origin of A-type silicic magma in the northern ANS included fractional crystallization of mantle-derived magma (Stern and Voegeli, 1995; Kessel et al., 1998; Jarrar et al., 2003) and melting of mafic lower crust (Jarrar et al., 1992, 2004). The new oxygen isotope data show that pure mantle origin of silicic magma is not possible, and a contribution of upper crustal, high- $\delta^{18}\text{O}$  sources to the rhyolite dyke magma is required. Therefore, if melting

of lower crust is considered, such crust should have included a significant component of protoliths that had been altered near the surface at low temperatures. A plethora of surface-derived rocks from earlier evolutionary stages of the ANS occur in southern Israel and should be considered as potential sources for the rhyolite magma. For example, melting of the peraluminous Elat granite thought to be derived from meta-sedimentary sources can account for the observed isotope ratios of the quartz porphyry [ $\delta^{18}\text{O}(\text{Zrn}) \sim 7\text{‰}$ ; Fig. 16; Eyal et al., 2004]. Melting of the late Proterozoic metamorphic upper crust represented by the Elat granitic gneiss [ $\delta^{18}\text{O}(\text{Zrn}) \sim 7\text{‰}$ ; Fig. 16] is also a possible scenario, which is supported by the Nd isotope data (Fig. 15). Thus, the role of mantle-derived magma in generating the quartz porphyry dykes was likely restricted to advection of heat with only subdued contribution of mafic material to the magma.

The recently acquired isotope data on the dykes of the bimodal suite and on some A-type granite plutons in the northern ANS give a new perspective on the long standing problem of the origin of the A-type granites (Loiselle and Wones, 1979; Collins et al., 1982; Whalen et al., 1987; Eby, 1990; Creaser et al., 1991; Turner et al., 1992; Kerr and Fryer, 1993; Wickham et al., 1995; Patiño Douce, 1997; Litvinovsky et al., 1999, 2002; Wu et al., 2002). In addition to the quartz porphyry dykes, appreciable crustal contribution is also indicated by the  $\delta^{18}\text{O}(\text{Zrn})$  values of the alkaline Yehoshafat granite, 6.52 to 6.76‰ (Fig. 16; Table 7). The granite formed in the beginning of the post-orogenic stage (Table 7) and is intruded by the bimodal dyke suite. In contrast to the relatively high oxygen isotope ratios of the rhyolitic

dykes and Yehoshafat granite, other A-type granites in the northern ANS bear a dominant mantle  $\delta^{18}\text{O}$  signature. In particular, the Timna alkaline granite pluton exposed  $\sim 20$  km to the north of the study area and also intruded by the bimodal dyke suite has average  $\delta^{18}\text{O}(\text{Zrn})$  of 5.52‰ (Table 7). Similar  $\delta^{18}\text{O}(\text{Zrn})$  values are obtained for syenogranite (5.81‰) and ring dyke perthite quartz syenite (5.48–5.66‰) from the alkaline Katharina ring complex (S. Sinai, Egypt) (Table 7). These values indicate that the generation of the alkaline granite magma involved either differentiation of mantle-derived alkaline mafic magma with minor assimilation of crustal material (Beyth et al., 1994) or melting of lower crust formed by underplating of K-rich basalt magma.

The abundant bimodal dyke swarms, A-type granite plutons and bimodal volcanic suites formed in an extensional tectonic environment (e.g., Stern, 1994; Garfunkel, 2000; Genna et al., 2002). Extension-induced ascent of mantle-derived mafic magma into the crust could either melt the existing continental crust and mix with the partial melts or merely result in fractional crystallization of mafic magma leading to granite formation (Eby, 1992; Black and Liégeois, 1993). The presence of two isotopically distinct groups of post-orogenic alkaline granite in the northern ANS, suggests that A-type magmatism may originate by alternative processes almost coevally.

## 8. Conclusions

1. The Late Pan-African bimodal dyke suite in southern Israel was formed by injection of alkaline rhyolitic and trachybasaltic magmas. Formation of composite dykes points to coexistence of silicic and mafic magmas.
2. Evidence of magma mixing is established. Mixing occurred both at shallow depth, in the process of formation of composite dykes, and at greater depth, still prior to dyke emplacement.
3. Dyke rocks have been subjected to extensive low-temperature alteration that caused significant disturbance of the magmatic  $^{18}\text{O}/^{16}\text{O}$  ratios in alkali feldspar and plagioclase. Magmatic  $^{18}\text{O}/^{16}\text{O}$  ratios in zircon, clinopyroxene and partly in quartz have been retained.
4. The Rb–Sr isotope ratios of the quartz porphyry are also dominated by low-temperature hydrous alteration process; hence they do not characterize the magmatic process.
5. Initial magmatic Nd isotope ratios were preserved in most rocks, and the  $\epsilon_{\text{Nd}}(T)$  values in mafic and felsic rocks overlap and range from  $\sim 1.2$  to 2.9. However,

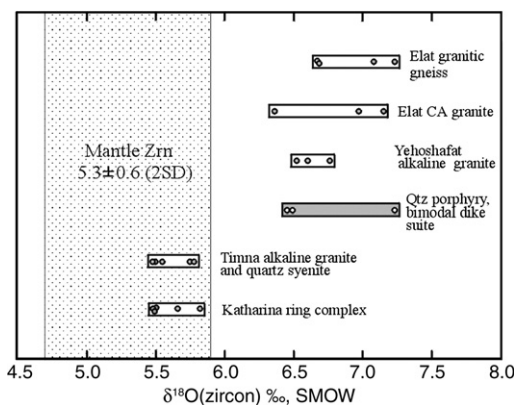


Fig. 16. Oxygen isotope ratios of zircon from igneous felsic rocks and granitic gneisses in southern Israel and the Sinai Peninsula (the Katharina ring complex). Two groups of A-type granites with different isotope signatures are distinguished. Mantle values of  $\delta^{18}\text{O}(\text{Zrn}) = 5.3 \pm 0.6$  ( $2\sigma$ ; Valley, 2003).

two sources of rhyolite melt are equally credible: K-rich basalt magma that produced coeval mafic dykes, and metamorphic rocks from the juvenile crust. Oxygen isotope ratios of zircon in quartz porphyry reveal significant crustal contribution to the rhyolites, suggesting that mafic and A-type silicic magmas are coeval, but not co-genetic.

6. Two groups of Late Neoproterozoic A-type granites are distinguished in the region: (1) those produced mostly from a mantle-derived source, with  $\delta^{18}\text{O}(\text{Zrn})$  ranging from 5.5 to 5.7‰ (Timna and Katharina granitoids), and (2) those with significant contribution of the modified juvenile crustal component, with  $\delta^{18}\text{O}(\text{Zrn})$  varying from 6.5 to 7.2‰ (Elat quartz porphyry dykes and Yehoshafat granite). This attests that A-type silicic magmas may originate by alternative processes almost coevally.

### Acknowledgements

This study was supported by the Ministry of National Infrastructure and Energy, Israel (grant #23-17-04), the Israel Science Foundation (grant 142/02) and by the National Science Council (NSC), Taiwan (grants NSC93-2116-M-001-025, NSC94-2116-M-001-021, NSC94-2752-M-002-010-PAE). Authors are greatly indebted to M. Beyth and an anonymous reviewer for valuable recommendations and corrections that provided a significant improvement to the paper.

### Appendix A. Supplementary data

Supplementary data associated with this article can be found, in the online version, at [doi:10.1016/j.lithos.2007.01.004](https://doi.org/10.1016/j.lithos.2007.01.004).

### References

- Agron, N., Bendor, Y.K., 1981. The volcanic massif of Biq'at Hayareah (Sinai–Negev), a case of potassium metasomatism. *J. Geol.* 89, 479–496.
- Baer, G., Beyth, M., Reches, Z., 1994. Dyke emplaced into fractured basement, Timna Igneous Complex, Israel. *J. Geophys. Res.* 99, 24039–24050.
- Baker, D.R., 1989. Tracer versus trace element diffusion: diffusional decoupling of Sr concentration from Sr isotope composition. *Geochim. Cosmochim. Acta* 53, 3015–3023.
- Baker, D.R., 1990. Chemical interdiffusion of dacite and rhyolite: anhydrous measurements at 1 atm and 10 kbar, application of transition state theory, and diffusion in zoned magma chambers. *Contrib. Mineral. Petrol.* 104, 407–423.
- Bendor, Y.K., 1985. The crust evolution of the Arabo-Nubian Massif with special reference to the Sinai Peninsula. *Precambrian Res.* 28, 1–74.
- Bendor, Y.K., Eyal, M., 1987. The geology of southern Sinai, its implication for the evolution of the Arabo-Nubian Massif. *Isr. Acad. Sci. Humanit., Jerusalem*.
- Beyth, M., Stern, R.J., Altherr, R., Kröner, A., 1994. The late Precambrian Timna igneous complex, Southern Israel: Evidence for comagmatic-type sanukitoid monzodiorite and alkali granite magma. *Lithos* 31, 103–124.
- Beyth, M., Longstaffe, F.J., Ayalon, A., Matthews, A., 1997. Epigenetic alteration of the Precambrian igneous complex at Mount Timna, southern Israel: oxygen-isotope studies. *Isr. J. Earth Sci.* 46, 1–11.
- Beyth, M., Heimann, A., 1999. The youngest igneous event in the crystalline basement of the Arabian–Nubian Shield, Timna Igneous Complex. *Isr. J. Earth Sci.* 48, 113–120.
- Bielski, M., 1982. Stages in the evolution of the Arabo-Nubian massif in Sinai. Ph.D. thesis, Hebrew Univ., Jerusalem (in Hebrew; English Abstract, Tables, Figures).
- Black, R., Liégeois, J.P., 1993. Cratons, mobile belts, alkaline rocks and continental lithospheric mantle: the Pan-African testimony. *J. Geol. Soc. (Lond.)* 150, 89–98.
- Carrigan, C.R., Eichelberg, J.C., 1990. Zoning of magmas by viscosity in volcanic conduits. *Nature* 343, 248–251.
- Cavosie, A.J., Valley, J.W., Wilde, S.A., E.I.M.F., 2005. Magmatic  $^{18}\text{O}$  in 4400–3900 Ma detrital zircons: a record of the alteration and recycling of crust in the early Archean. *Earth Planet. Sci. Lett.* 235, 663–681.
- Chiba, H., Chacko, T., Clayton, R.N., Goldsmith, J.R., 1989. Oxygen isotope fractionations involving diopside, forsterite, magnetite and calcite: application to geothermometry. *Geochim. Cosmochim. Acta* 53, 2895–2995.
- Clayton, R.N., Goldsmith, J.R., Mayeda, T.K., 1989. Oxygen isotope fractionation in quartz, albite, anorthite and calcite. *Geochim. Cosmochim. Acta* 53, 725–733.
- Collins, W.J., Beams, S.D., White, A.J.R., Chappell, B.W., 1982. Nature and origin of A-type granites with particular reference to Southeastern Australia. *Contrib. Mineral. Petrol.* 80, 189–200.
- Creaser, R.A., Price, R.C., Wormald, R.J., 1991. A-type granites revisited: assessment of a residual-source model. *Geology* 19, 63–166.
- Criss, R.E., Taylor, H.P., 1983. An  $^{18}\text{O}/^{16}\text{O}$  and D/H study of Tertiary hydrothermal systems in the southern half of the Idaho batholith. *Geol. Soc. Amer. Bull.* 94, 640–663.
- Criss, R.E., Taylor, H.P., 1986. Meteoric-hydrothermal systems. In: Valley, J.W., Taylor, H.P., O'Neil, J.R. (Eds.), *Stable Isotopes in High Temperature Geological Processes. Reviews in Mineralogy*, vol. 16. Mineral. Soc. America, Washington, DC, pp. 373–424.
- DePaolo, D.J., 1988. Neodymium Isotope Geochemistry: An Introduction. Springer-Verlag, New York.
- Eby, G.N., 1990. The A-type granitoids: a review of their occurrence and chemical characteristics and speculations on their petrogenesis. *Lithos* 26, 115–134.
- Eby, G.N., 1992. Chemical subdivision of the a-type granitoids: petrogenetic and tectonic implications. *Geology* 20, 641–644.
- Eiler, J.M., Farley, K.A., Valley, J.W., Hofmann, A.W., Stolper, E.M., 1996. Oxygen isotope constraints on the sources of Hawaiian volcanism. *Earth Planet. Sci. Lett.* 144, 453–468.
- Eiler, J.M., Crawford, A., Elliott, T., Farley, K.A., Valley, J.W., Stolper, E.M., 2000. Oxygen isotope geochemistry of oceanic-arc lavas. *J. Petrol.* 41, 229–256.
- Eyal, M., Hezkiyahu, T., 1980. Katharina Pluton — the outlines of a petrological framework. *Isr. J. Earth Sci.* 29, 41–52.
- Eyal, Y., Eyal, M., Kröner, A., 1991. Geochronology of the Elat Terrain metamorphic basement, and its implication for crustal

- evolution of the NE part of the Arabian–Nubian Shield. *Isr. J. Earth Sci.* 40, 5–16.
- Eyal, M., Litvinovsky, B.A., Katzir, Y., Zanvilevich, A.N., 2004. The Pan-African high-K calc-alkaline peraluminous Elat granite of southern Israel: geology, geochemistry and petrogenesis. *J. Afr. Earth Sci.* 40, 115–136.
- Furman, T., Spera, F.J., 1985. Co-mingling of acid and basic magma with the implications for the origin of mafic I-type xenoliths: field and petrochemical relations of an unusual dike complex at Eagle Lake, Sequoia National Park, California, USA. *J. Volcanol. Geotherm. Res.* 24, 151–178.
- Furnes, H., El-Sayed, M.M., Khalil, S.O., Hassanen, M.A., 1996. Pan-African magmatism in the Wadi El-Imra district, Central Eastern Desert, Egypt: geochemistry and tectonic environment. *J. Geol. Soc. (Lond.)* 153, 705–718.
- Gal, A., 2006. Oxygen Isotope Perspective on Post-Orogenic Alkaline Magmatism in the Arabian–Nubian Shield of Southern Israel. MS thesis, Ben-Gurion University of the Negev, Be'er Sheva, Israel, (in Hebrew; English Abstract).
- Garfunkel, Z., 2000. History and paleogeography during the Pan-African orogen to stable platform transition: Reappraisal of the evidence from Elat area and the northern Arabian–Nubian Shield. *Isr. J. Earth Sci.* 48, 135–157.
- Garfunkel, Z., Eyal, Y., Eyal, M., Weissbrod, T., Bakler, N., Shimron, A.E., Peltz, S., Gutkin, V., Bartov, Y., Drukman, Y., Rozenfeld, M., Sneh, A., 2000. Geological map of the Northern Gulf of Elat area, scale 1:100,000 (sheet 26 Elat). *Geol. Surv. Isr.*, Jerusalem.
- Genna, A., Nehlig, P., Le Goff, E., Guerrot, C., Shanti, M., 2002. Proterozoic tectonism of the Arabian Shield. *Precambrian Res.* 117, 21–40.
- Gibson, I.L., Walker, G.P.L., 1963. Some composite rhyolite/basalt lavas and related composite dikes in eastern Iceland. *Proc. Geol. Assoc.* 74, 301.
- Gutkin, V., Eyal, Y., 1998. Geology and evolution of Precambrian rocks, Mt. Shelomo, Elat area. *Isr. J. Earth Sci.* 47, 1–18.
- Iacumin, M., Mazaroli, A., El-Metwally, A.A., Piccirillo, E.M., 1998. Neoproterozoic dyke swarms from southern Sinai (Egypt): geochemistry and petrogenetic aspects. *J. Afr. Earth Sci.* 26, 49–64.
- Jarrar, G., 2001. The youngest Neoproterozoic mafic dike suite in the Arabian Shield: mildly alkaline dolerites from South Jordan — their geochemistry and petrogenesis. *Geol. Mag.* 138, 309–323.
- Jarrar, G., Wachendorf, H., Saffarini, G., 1992. A Late Proterozoic bimodal volcanic/subvolcanic suite from Wadi Araba, southwest Jordan. *Precambrian Res.* 56, 51–72.
- Jarrar, G., Stern, R.J., Saffarini, G., Al-Zubi, H., 2003. Late and post-orogenic Neoproterozoic intrusions of Jordan: implications for crustal growth in the northernmost segment of the East African Orogen. *Precambrian Res.* 123, 295–319.
- Jarrar, G., Saffarini, G., Baumann, A., Wachendorf, H., 2004. Origin, age and petrogenesis of Neoproterozoic composite dikes from the Arabian–Nubian Shield, SW Jordan. *Geol. J.* 39, 157–178.
- Kanaris-Sotiriou, R., Gill, F.G.F., 1985. Hybridization and the petrogenesis of composite intrusions: The dike at An Cumhann, Isle of Arran, Scotland. *Geol. Mag.* 122, 361–372.
- Katzir, Y., Litvinovsky, B.A., Eyal, M., Zanvilevich, A.N., Vapnik, Ye., 2006. Four successive episodes of Late Pan-African dykes in the central Elat area, southern Israel. *Isr. J. Earth Sci.* 55 (2).
- Katzir, Y., Eyal, M., Litvinovsky, B.A., Jahn, B.-M., Zanvilevich, A.N., Valley, J.W., Beeri, Y., Pelly, I., Shimshilashvili, E., 2007. Petrogenesis of A-type granites and origin of vertical zoning in the Katharina pluton, area of Gebel Mussa (Mt. Moses), Sinai, Egypt. *Lithos.* 95, 208–228.
- Kerr, A., Fryer, B.J., 1993. Nd isotope evidence for crust–mantle interaction in the generation of A-type granitoid suites in Labrador, Canada. *Chem. Geol.* 104, 39–60.
- Kessel, R., Stein, M., Navon, O., 1998. Petrogenesis of late Neoproterozoic dikes in the northern Arabian–Nubian Shield. Implication for the origin of A-type granites. *Precambrian Res.* 92, 195–213.
- Keto, L.S., Jacobsen, S.B., 1987. Nd and Sr isotopic variations of Early Paleozoic oceans. *Earth Planet. Sci. Lett.* 84, 27–41.
- King, E.M., Valley, J.W., Davis, D.W., Edwards, G.R., 1998. Oxygen isotope ratios of Archean plutonic zircons from granite–greenstone belts of the Superior Province: indicator of magmatic source. *Precambrian Res.* 92, 365–387.
- Koyaguchi, T., Takada, A., 1994. An experimental study of the formation of composite intrusions from zoned magma chambers. *J. Volcanol. Geotherm. Res.* 59, 261–267.
- Lasher, C.E., 1990. Decoupling of chemical and isotopic exchange during magma mixing. *Nature* 344, 235–237.
- Lasher, C.E., 1994. Kinetics of Sr and Nd exchange in silicate liquids: theory, experiments, and applications to uphill diffusion, isotopic equilibration and irreversible mixing of magmas. *J. Geophys. Res.* 99, 9585–9604.
- Liégeois, J.-P., Black, R., 1987. Alkaline magmatism subsequent to collision in the Pan-African belt of the Adrar des Iforas. In: Fitton, J.G., Upton, B.G.J. (Eds.), *Alkaline Igneous Rocks*. *Geol. Soc. Spec. Publ.*, vol. 30, pp. 381–401.
- Litvinovsky, B.A., Zanvilevich, A.N., Kalmanovich, M.A., 1995a. Recurrent mixing and mingling of coexisting syenite and basalt magmas in the Ust'-Khilok massif, Transbaikalia, and its petrologic significance. *Petrology* 3, 115–137.
- Litvinovsky, B.A., Zanvilevich, A.N., Lyapunov, S.M., Bindeman, I.N., Davis, A.M., Kalmanovich, M.A., 1995b. Model of composite basite-granitoid dike generation (Shaluta Pluton, Transbaikalia). *Russ. Geol. Geophys.* 36, 1–19.
- Litvinovsky, B.A., Zanvilevich, A.N., Wickham, S.M., Steele, I.M., 1999. Origin of syenitic magmas from anorogenic granitoid series: syenite–granite series from Transbaikalia. *Petrology (Moscow)* 7, 483–508.
- Litvinovsky, B.A., Jahn, B.-M., Zanvilevich, A.N., Saunders, A., Poulain, S., 2002. Petrogenesis of syenite–granite suites from the Bryansky Complex (Transbaikalia, Russia): implications for the origin of A-type granitoid magmas. *Chem. Geol.* 189, 105–133.
- Litvinovsky, B.A., Eyal, M., Zanvilevich, A.N., Katzir, Y., Jahn B.-M., Beeri, Y., Valley, J.W., Vapnik, Ye., in press. Late Neoproterozoic dykes in the northernmost Arabian–Nubian shield (southern Israel): sequence of dyke episodes, geochemical and isotope evidence of magma sources. Submitted to *Int. J. Earth Sci.*
- Loiselle, M.C., Wones, D.R., 1979. Characteristics and origin of anorogenic granites. *Geol. Soc. Am. Abstr. Progr.* 11, 468.
- Macpherson, C.G., Gamble, J.A., Matthey, D.P., 1998. Oxygen isotope geochemistry of lavas from an oceanic to continental arc transition, Kermadec–Hikurangi margin, SW Pacific. *Earth Planet. Sci. Lett.* 160, 609–621.
- Marco, S., Ron, H., Matthews, A., Beyth, M., Navon, O., 1993. Chemical remanent magnetism related to the Dead Sea Rift: Evidence from Precambrian igneous rock of mount Timna, southern Israel. *J. Geophys. Res.* 98, 16001–16012.
- Marian, P.D., Piccoli, P.P.M., 1989. Tectonic discrimination of granitoids. *Geol. Soc. Amer. Bull.* 101, 635–643.

- Marshall, L.A., Sparks, R.S.J., 1984. Origin of some mixed-magma and net-veined ring intrusions. *J. Geol. Soc. (Lond.)* 141, 171–182.
- Mattey, D., Lowry, D., Macpherson, C., 1994a. Oxygen isotope composition of mantle peridotite. *Earth Planet. Sci. Lett.* 128, 231–241.
- Mattey, D., Lowry, D., Macpherson, C., Chazot, G., 1994b. Oxygen isotope composition of mantle minerals by laser fluorination analysis: homogeneity in peridotites, heterogeneity in eclogites. *Mineral. Mag.* 58A, 573–574.
- Matthews, A., Ayalon, A., Ziv, A., Shaked, J., 1999. Hydrogen and oxygen isotope studies of alteration in the Timna igneous complex. *Isr. J. Earth Sci.* 48, 121–131.
- Moghazi, A.M., 2002. Petrology and geochemistry of Pan-African granitoids, Kab Amiri area, Egypt — implications for tectonomagmatic stages of the Nubian Shield evolution. *Mineral. Petrol.* 75, 41–67.
- Mushkin, A., Navon, O., Halicz, L., Heimann, A., Wöerner, G., Stein, M., 1999. Geology and geochronology of the Amram Massif rocks, southern Negev Desert, Israel. *Isr. J. Earth Sci.* 48, 179–193.
- Mushkin, A., Navon, O., Halicz, L., Heimann, A., Hartmann, G., Stein, M., 2003. The petrogenesis of A-type magmas from the Amram Massif, southern Israel. *J. Petrol.* 44, 815–832.
- Page, F.Z., Deangelis, M., Fu, B., Kita, N., Lancaster, P., Valley J.W., 2006. Slow oxygen diffusion in zircon. 16th V.M. Goldschmidt Conference, Melbourne, Australia. Abstracts.
- Patiño Douce, A.E., 1997. Generation of metaluminous A-type granites by low-pressure melting of calc-alkaline granitoids. *Geology* 25, 743–746.
- Pearce, J.A., Cann, J.R., 1973. Tectonic setting of basic volcanic rocks determined using trace element analyses. *Earth Planet. Sci. Lett.* 19, 290–300.
- Pearce, J.A., Harris, N.B., Tindle, A.G., 1984. Trace element discrimination diagrams for the tectonic interpretation of granitic rocks. *J. Petrol.* 25, 956–983.
- Peck, W.H., King, E.M., Valley, J.W., 2000. Oxygen isotope perspective on Precambrian crustal growth and maturation. *Geology* 28, 363–366.
- Poli, G.E., Tommazzini, S., 1991. Model of the origin and significance of microgranular enclaves in calc-alkaline granitoids. *J. Petrol.* 32, 657–666.
- Snyder, D., Crambles, C., Tait, S., Wiebe, R.A., 1997. Magma mingling in dikes and sills. *J. Geol.* 105, 75–86.
- Snyder, D., Tait, S., 1998. The imprint of basalt on the geochemistry of silicic magmas. *Earth Planet. Sci. Lett.* 160, 433–445.
- Spicuzza, M.J., Valley, J.W., Kohn, M.J., Girard, J.P., Fouillac, A.M., 1998a. The rapid heating, defocused beam technique: a CO<sub>2</sub>-laser-based method for highly precise and accurate determination of  $\delta^{18}\text{O}$  values of quartz. *Chem. Geol.* 144, 195–203.
- Spicuzza, M.J., Valley, J.W., McConnell, V.S., 1998b. Oxygen isotope analysis of whole rock via laser fluorination: an air-lock approach. *Geol. Soc. Am. Abstr. Progr.* 30, 80.
- Stein, M., 2003. Tracing the plume material in the Arabian–Nubian Shield. *Precambrian Res.* 123, 223–234.
- Stein, M., Hoffman, A.W., 1992. Fossil plumes beneath the Arabian lithosphere? *Earth Planet. Sci. Lett.* 114, 193–209.
- Stein, M., Goldstein, S.L., 1996. From plume head to continental lithosphere in the Arabian–Nubian shield. *Nature* 382, 773–778.
- Stein, M., Navon, O., Kessel, R., 1997. Chromatographic metasomatism of the Arabian–Nubian lithosphere. *Earth Planet. Sci. Lett.* 152, 75–91.
- Stern, R.J., 1994. Arc assembly and continental collision in the Neoproterozoic East African orogen. Implications for the consolidation of Gondwanaland. *Annu. Rev. Earth Planet. Sci.* 22, 319–351.
- Stern, R.J., 2002. Crustal evolution in the East African Orogen: a neodymium isotopic perspective. *J. Afr. Earth Sci.* 34, 109–117.
- Stern, R.J., Gottfried, D., Hedge, C.E., 1984. Late Precambrian rifting and crustal evolution in the North Eastern Desert of Egypt. *Geology* 12, 168–172.
- Stern, R.J., Hedge, C.E., 1985. Geochronologic and isotopic constraints on Late Precambrian crustal evolution in the Eastern Desert of Egypt. *Am. J. Sci.* 285, 97–127.
- Stern, R.J., Gottfried, D., 1986. Petrogenesis of the Late Precambrian (575–600 Ma) bimodal suite in the Northeast Africa. *Contrib. Mineral. Petrol.* 92, 492–501.
- Stern, R.J., Voegeli, D.F., 1987. Geochemistry, geochronology, and petrogenesis of a Late Precambrian (=590 Ma) composite dike from the North Eastern Desert of Egypt. *Geol. Rundsch.* 76, 325–341.
- Stern, R.J., Sellers, G., Gottfried, D., 1988. Bimodal dike swarms in the North of the Eastern Desert of Egypt: Significance for the origin of the Precambrian “A-type” Granites in Northern Afro-Arabia. In: Greiling, R., Gaby, R. (Eds.), *The Pan-African Belt of NE Africa and Adjacent Areas: Tectonic Evolution and Economic Aspects*. Frieder. Vieweg. and Sohn, Braunschweig, Germany, pp. 147–179.
- Stern, R.J., Kröner, A., 1993. Late Precambrian crustal evolution in NE Sudan, isotopic and geochronologic constraints. *J. Geol.* 101, 555–574.
- Stern, R.J., Voegeli, D., 1995. Late Neoproterozoic (570 Ma) composite dykes from the Northern Arabian–Nubian Shield: Petrogenetic perspectives on contemporaneous mafic and felsic igneous activity. Third international Dyke Conference, Jerusalem, September 4–8, 1995, p. 69. Abstracts.
- Stern, R.J., Abdelsalam, M.G., 1998. Formation of continental crust in the Arabian–Nubian Shield: evidence from granitic rocks of the Nakasib suture, NE Sudan. *Geol. Rundsch.* 87, 150–160.
- Stoeser, D.B., Camp, V.E., 1985. Pan-African microplate accretion of Arabian shield. *Geol. Soc. Amer. Bull.* 96, 817–826.
- Sun, S., McDonough, W.F., 1989. Chemical and isotopic systematics of oceanic basalts: implications for mantle compositions and processes. In: Saunders, A.D., Norry, M.J. (Eds.), *Magmatism in the Ocean Basins*. *Geol. Soc. Spec. Publ.*, vol. 42, pp. 313–345.
- Sylvester, P.J., 1989. Post-collisional alkaline granites. *J. Geol.* 97, 261–281.
- Titov, A.V., Litvinovsky, B.A., Zavnilevich, A.N., Shadaev, M.G., 2000. Hybridization in composite basic-rock-leucogranite dikes of the Ust'-Khilol massif, Transbaikalia. *Russ. Geol. Geophys.* 41, 1662–1675.
- Turner, S.P., Foden, J.D., Morrison, R.S., 1992. Derivation of some A-type magmas by fractionation of basaltic magma: an example from the Padthway Ridge, South Australia. *Lithos* 28, 151–179.
- Valley, J.W., 2003. Oxygen isotopes in zircon. In: Hanchar, J.M., Hoskin, W.O. (Eds.), *Zircon. Reviews in Mineralogy and Geochemistry*, vol. 53. Mineral. Soc. America, Washington, DC, pp. 343–385.
- Valley, J.W., Chiarenzelli, J.R., McLelland, J.M., 1994. Oxygen isotope geochemistry of zircon. *Earth Planet. Sci. Lett.* 126, 187–206.
- Valley, J.W., Kitchen, N., Kohn, M.J., Niendorf, C.R., Spicuzza, M.J., 1995. UWG-2, a garnet standard for oxygen isotope ratios: strategies for high precision and accuracy with laser heating. *Geochim. Cosmochim. Acta* 59, 5523–5531.
- Valley, J.W., Bindeman, I.N., Peck, W.H., 2003. Empirical calibration of oxygen isotope fractionation in zircon. *Geochim. Cosmochim. Acta* 67, 3257–3266.

- Valley, J.W., Lackey, J.S., Cavosie, A.J., Clechenko, C.C., Spicuzza, M.J., Basei, M.A.S., Bindeman, I.N., Ferreira, V.P., Sial, A.N., King, E.M., Peck, W.H., Sinha, A.K., Wei, C.S., 2005. 4.4 billion years of crustal maturation: oxygen isotopes in magmatic zircon. *Contrib. Mineral. Petrol.* 150, 561–580.
- Vogel, T.A., Wilband, J.T., 1978. Coexisting acidic and basic melts: geochemistry of a composite dike. *J. Geol.* 86, 353–371.
- Wachendorf, H., Zachmann, D., Jarrar, G.H., 1985. The role of pressure in control of potassium, sodium, and copper concentration in hypabyssal intrusives as demonstrated in Late Precambrian dikes in southern Jordan. *Precambrian Res.* 30, 221–248.
- Wenner, D.B., Taylor Jr., 1976. Oxygen and hydrogen isotope studies of Precambrian granite–rhyolite terrane, St. Francois Mountains, southeastern Missouri. *Geol. Soc. Amer. Bull.* 87, 1587–1598.
- Whalen, J.B., Currie, K.L., Chappé, B.W., 1987. A-type granites: geochemical characteristics, discrimination and petrogenesis. *Contrib. Mineral. Petrol.* 95, 407–419.
- Wickham, S.M., Litvinovsky, B.A., Zanzvilevich, A.N., Bindeman, I.N., 1995. Geochemical evolution of Phanerozoic magmatism in Transbaikalia, East Asia: a key constraint of the origin of K-rich silicic magmas and the process of cratonization. *J. Geophys. Res.* 100/B8, 15641–15654.
- Wiebe, R.A., Ulrich, R., 1997. Origin of composite dikes in the Gouldsboro granite, coastal Maine. *Lithos* 40, 157–178.
- Winchester, J.A., Floyd, P.A., 1977. Geochemical discrimination of different magma series and their differentiation products using immobile elements. *Chem. Geol.* 70, 319–339.
- Wu, F.-Y., Sun, D.-Y., Li, H.-M., Jahn, B.-M., Wilde, S.A., 2002. A-type granites in Northeastern China: age and geochemical constraints on their petrogenesis. *Chem. Geol.* 187, 143–173.
- Zorpi, M.J., Couloh, C., Orsini, J.B., 1991. Hybridization between felsic and mafic magmas in calc-alkaline granitoids — a case study in northern Sardinia, Italy. *Chem. Geol.* 92 (1/3), 45–86.